(Supplementary Information)

Discovery, Validation, and Exploration of Mechanistically Distinct FtsZ Compounds Inhibiting Mycobacterial Cell Division

Jinglan Wang[1#], Qiping Hu[1#], Heng Wang[1], Genhui Xiao[1], Heli Jiang[1], Yueyang Xu[1], Yu Chang[1], Miaomiao Pan[1], Mengyun Zhang[1], Liangliang Zhou[1], E Liang[1], Yuan Zhang[1], Ruiyuan Liu[2], Jinzhi Wu[1], C.K. Chan[1], Jinjiang Guo[1], Renhe Liu[1], Lan Xu[1], Zhiyang Zou[1], Rumin Zhang[1], Yu Lu[3], Tanya Parish[4], Junhao Zhu[2]*, Shawn Chen[1]*

[1]Global Health Drug Discovery Institute, Haidian, Beijing 100192, China

[2]Laboratory of Pathogen Microbiology and Immunology, Institute of Microbiology, Chinese Academy of Sciences, Beijing, China

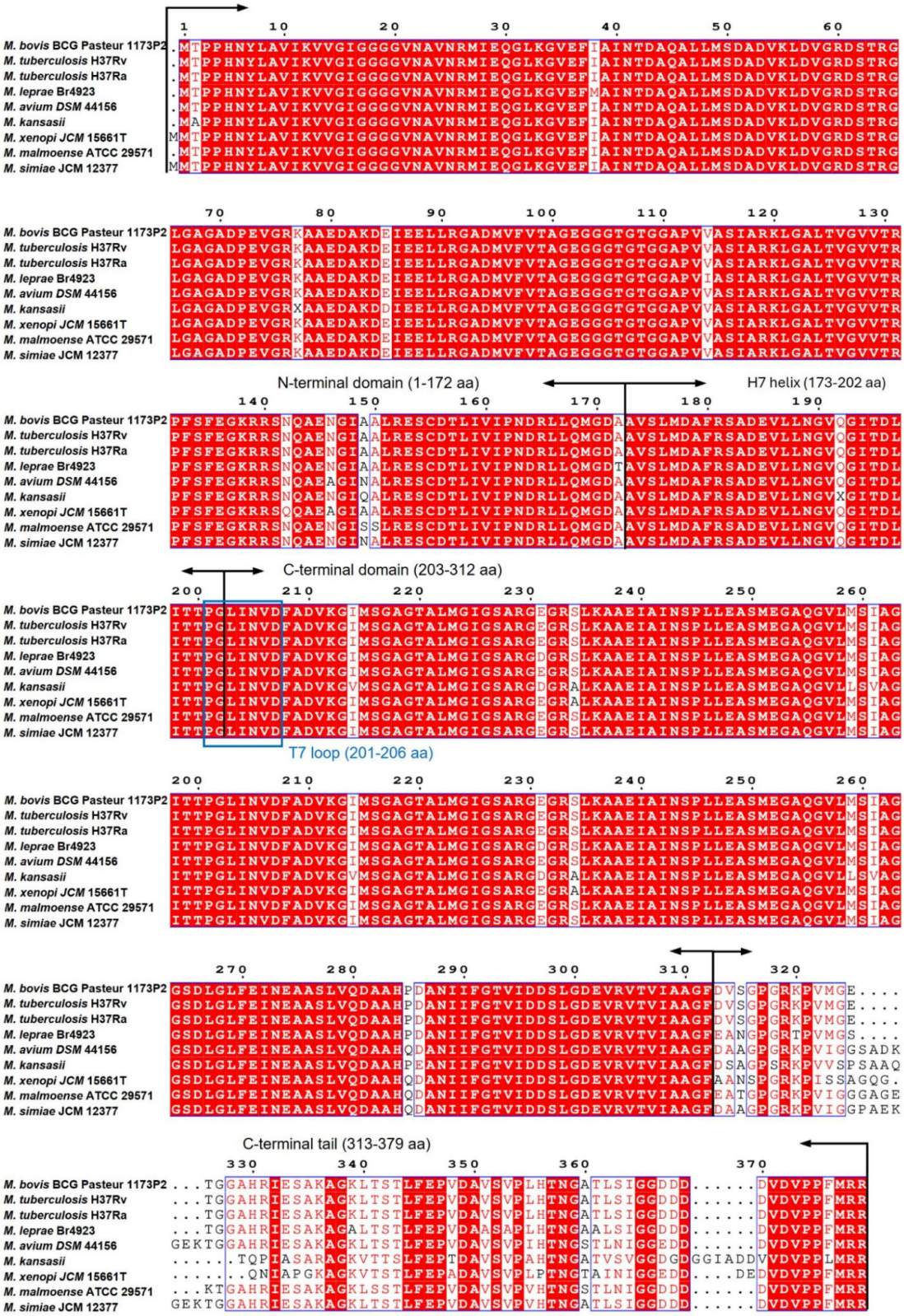
[3]Beijing Key Laboratory of Drug Resistance Tuberculosis Research, Beijing Chest Hospital, and Capital Medical University, Beijing, China

[4]Department of Tropical Disease Biology, Liverpool School of Tropical Medicine, Pembroke Place, Liverpool, L3 5QA, UK

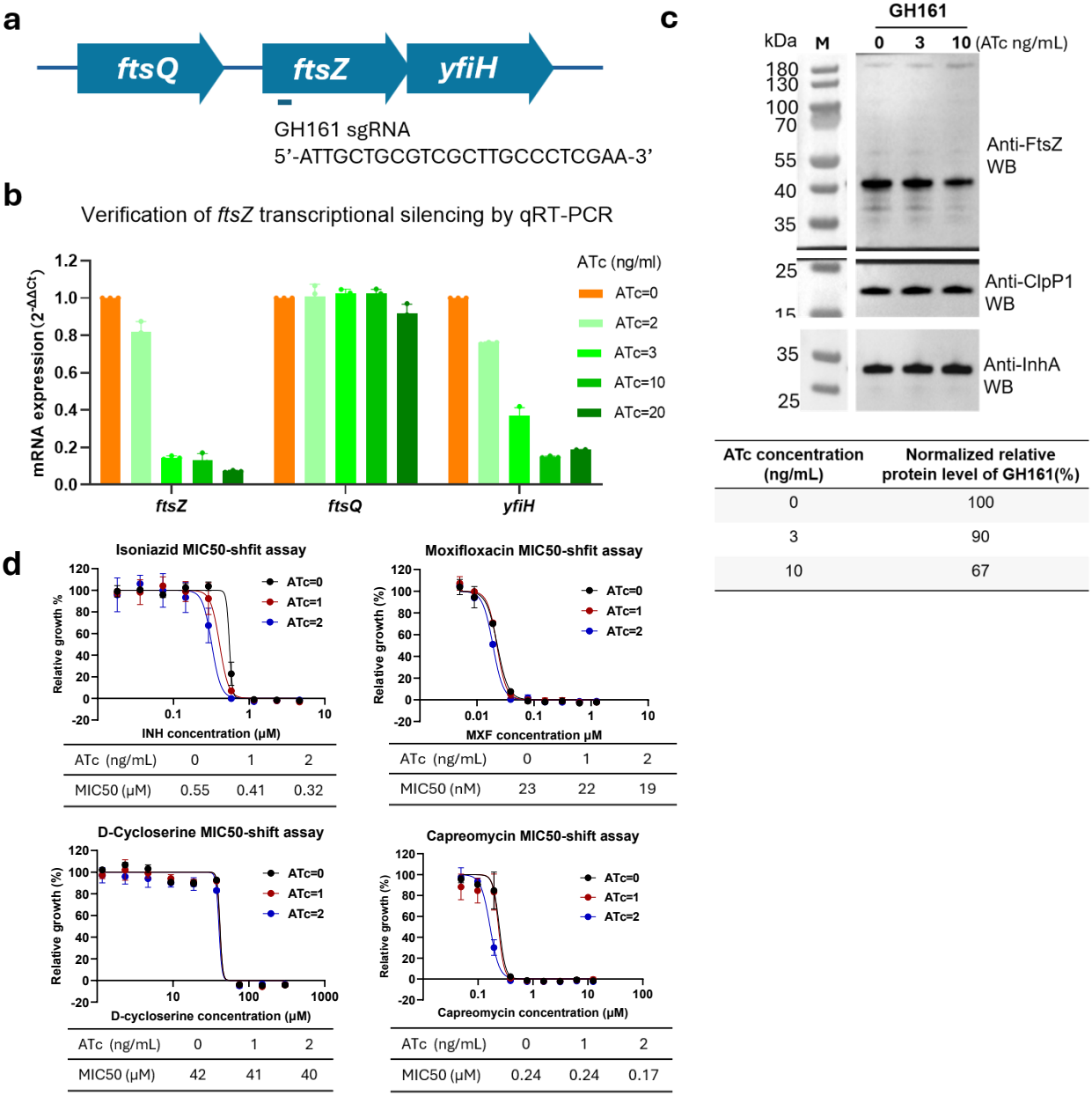
[#]These authors contributed equally

*Co-correspondence:

Junhao Zhu (zhujh@im.ac.cn) and Shawn Chen (shuo.chen@ghddi.org)



Supplementary Figure 1. FtsZ sequence alignment. The domains and structural features are annotated.



ATc concentration (ng/mL)	Normalized relative protein level of GH161(%)
0	100
3	90
10	67

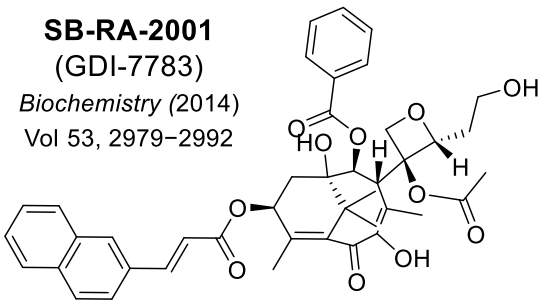
ATc (ng/mL)	0	1	2
MIC50 (μM)	0.55	0.41	0.32

ATc (ng/mL)	0	1	2
MIC50 (nM)	23	22	19

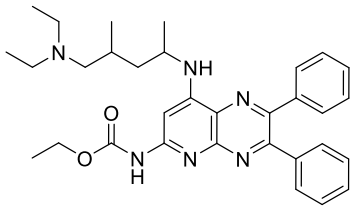
ATc (ng/mL)	0	1	2
MIC50 (μM)	42	41	40

ATc (ng/mL)	0	1	2
MIC50 (μM)	0.24	0.24	0.17

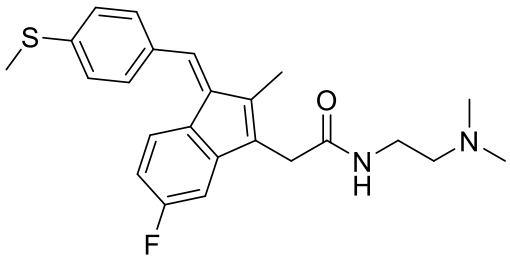
Supplementary Figure 2. Construction and validation of the *ftsZ* knockdown strain GH161. (**a**) Genomic organization of the *ftsZ* locus in BCG and location of the sgRNA expressed from an anhydrotetracycline (ATc) inducible promoter on a plasmid to repress *ftsZ* transcription. The downstream open reading frame (*yfiH*) appears to be transcribed from the same promoter as *ftsZ*, whereas a 172-bp intergenic region separates *ftsZ* from the upstream gene *ftsQ*. (**b**) Quantitative reverse-transcription PCR analysis of *ftsZ* mRNA levels in GH161 after 2 days of induction by the indicated concentrations of anhydrotetracycline (ATc). Relative transcript levels of *ftsZ*, *ftsQ*, and *yfiH* were normalized to the housekeeping genes *rpoB* and 16S rRNA. The experiment was performed twice with three biological replicates per condition; error bars indicate standard errors. (**c**) Western blot (WB) analysis of FtsZ protein levels in GH161 after 48 h of exposure to the indicated ATc concentrations. ClpP1 and InhA served as internal reference proteins. Relative FtsZ abundance was quantified from the Western blots using ImageJ and normalized to the reference condition. (**d**) Chemical-genetic interactions between anti-TB drugs and the *ftsZ*-KD in GH161 were demonstrated with Isoniazid, Moxifloxacin, D-Cycloserine, and Capreomycin.



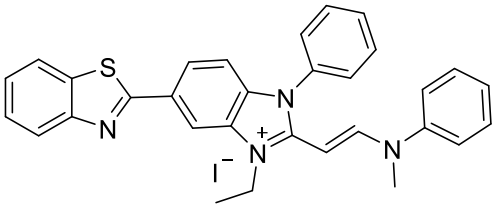
SB-RA-2001
(GDI-7783)
*Biochemistry (*2014)
Vol 53, 2979−2992



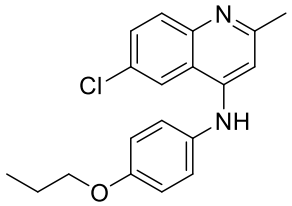
SRI-3072
(MMV 1633967)
J Antimicro Chemo (2002) Vol 50, 111–114



Sulindac sulfide derivative-18
PLoS ONE (2016) Vol 11, e0164100

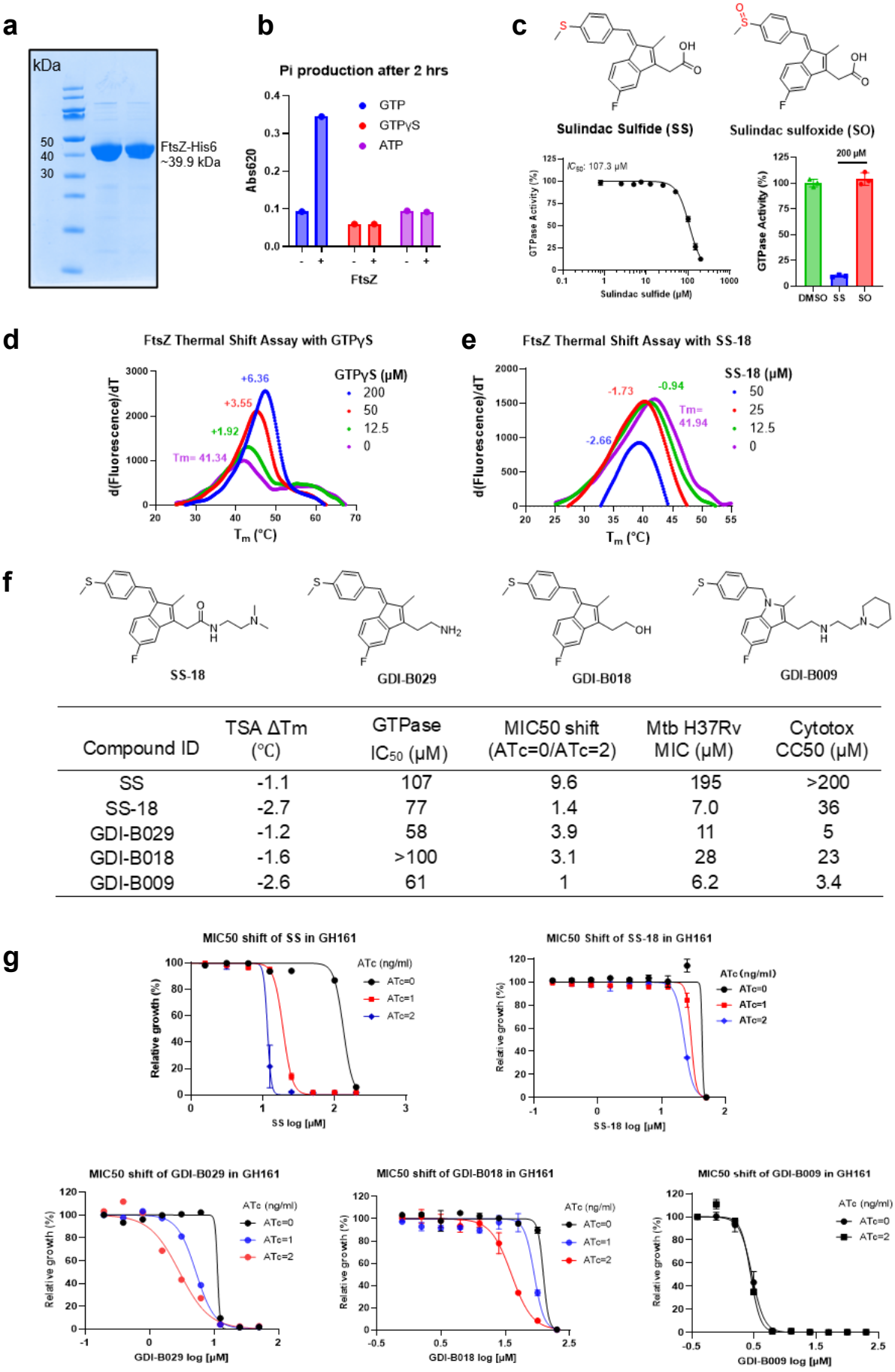


Zantrin Z2
PNAS (2004) Vol 101, 11821–11826



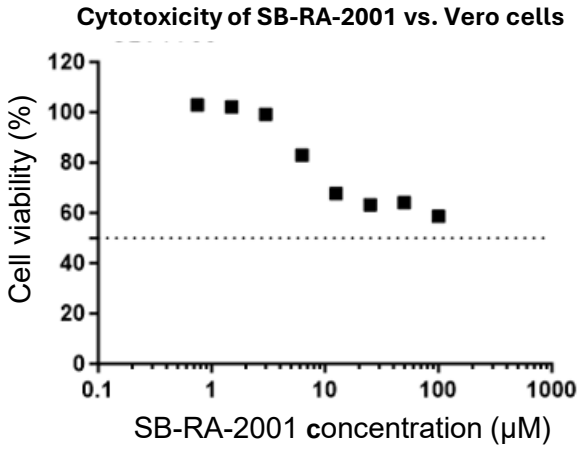
Quinoline-1
Tuberculosis (2013) Vol 93, 398-400

Supplementary Figure 3. Structures, compound identifiers, and literature references for a few reported anti-TB FtsZ inhibitors. Assay data for the five compounds, obtained in our experiments, are summarized in Table 1.

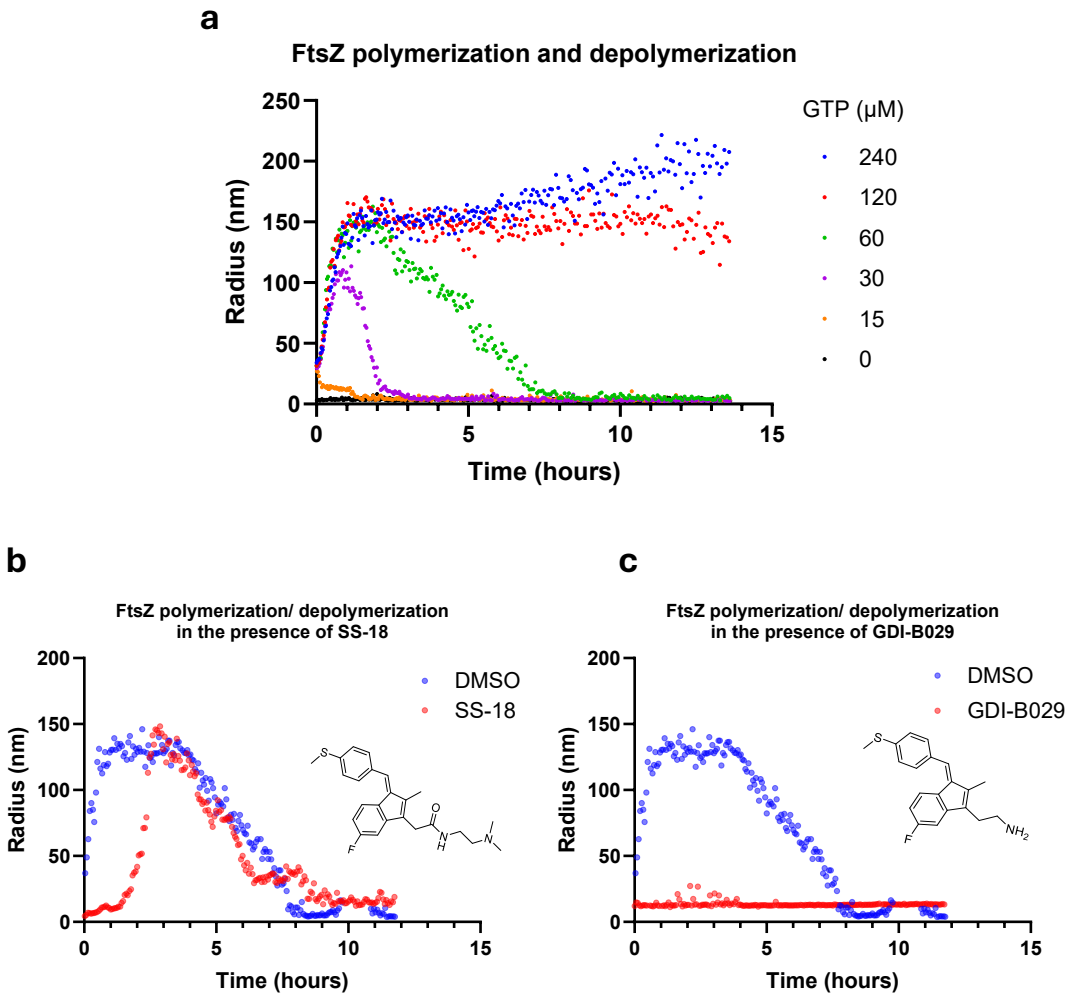


Compound ID	TSA ΔTm (℃)	GTPase IC_{50} (μM)	MIC50 shift (ATc=0/ATc=2)	Mtb H37Rv MIC (μM)	Cytotox CC50 (μM)
SS	-1.1	107	9.6	195	>200
SS-18	-2.7	77	1.4	7.0	36
GDI-B029	-1.2	58	3.9	11	5
GDI-B018	-1.6	>100	3.1	28	23
GDI-B009	-2.6	61	1	6.2	3.4

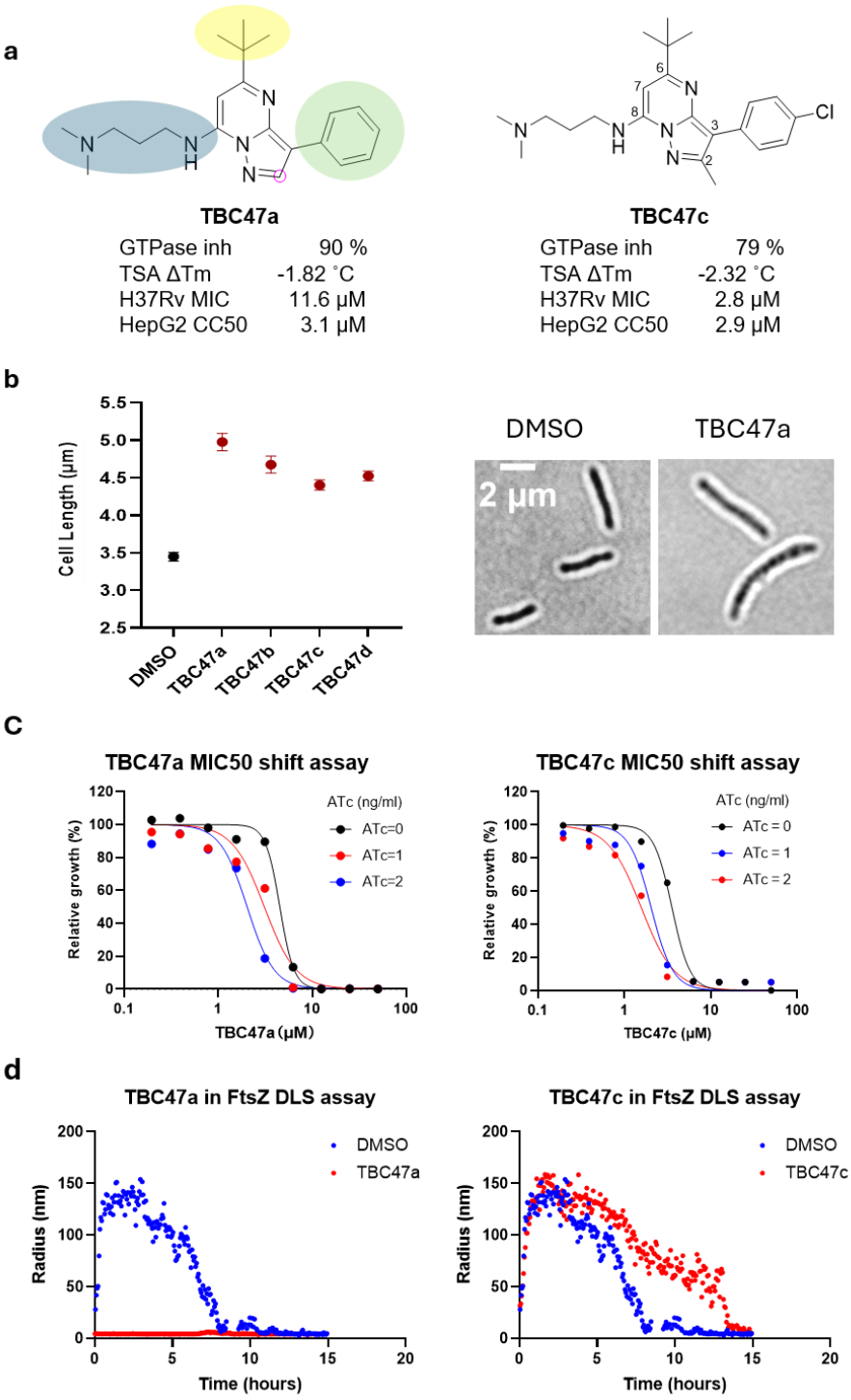
Supplementary Figure 4. Development of biochemical assays for MtbFtsZ using sulindac sulfide derivatives and validation of the series with CRISPRi *ftsZ*-KD mutant. (**a, b**) GTPase inhibition assay. Purified MtbFtsZ bearing a cleavable affinity tag hydrolyzes GTP and releases inorganic phosphate, which was quantified using malachite green. MtbFtsZ did not hydrolyze ATP or the nonhydrolyzable GTP analog GTPγS. Because MtbFtsZ has a relatively low GTPase activity and slowly growing mycobacteria have a doubling time of approximately 20 h, reactions were incubated for at least 2 h and, in some experiments, up to 16 h. The repurposed drug sulindac has been reported to inhibit MtbFtsZ[1]. (**c**) Sulindac sulfide (SS) and sulindac sulfoxide (SO) were tested in the assay. SO was inactive at 200 μM, whereas SS inhibited MtbFtsZ GTPase activity with an IC50 of ~107.3 μM. Experimental conditions are provided in the Methods. (**d, e**) Thermal shift assay (TSA), also known as differential scanning fluorimetry (DSF)[2–4], was used to assess the effects of ligand binding on the thermal stability of purified MtbFtsZ. MtbFtsZ was monitored using Sypro Orange. The nonhydrolyzable GTP analog GTPγS stabilized MtbFtsZ and produced a positive shift in melting temperature (T_m), whereas SS-18 destabilized the protein and produced a concentration-dependent negative thermal shift. (**f**) Structures and biochemical assay results for sulindac sulfide-derived analogs. The table is presented in the same format as Table 1. (**g**) Cellular target engagement was assessed using the MIC50-shift assay in GH161 cells induced for *ftsZ* knockdown. Although several thermally destabilizing compounds potently inhibited MtbFtsZ in vitro, their cellular activity was attributable only partly to FtsZ inhibition like SS-18 and was not clearly attributable to FtsZ inhibition like GDI-B009. In contrast, the large MIC50 shift observed for the SS supported its cellular engagement of MtbFtsZ. The SS analogs showed increased cytotoxicity.



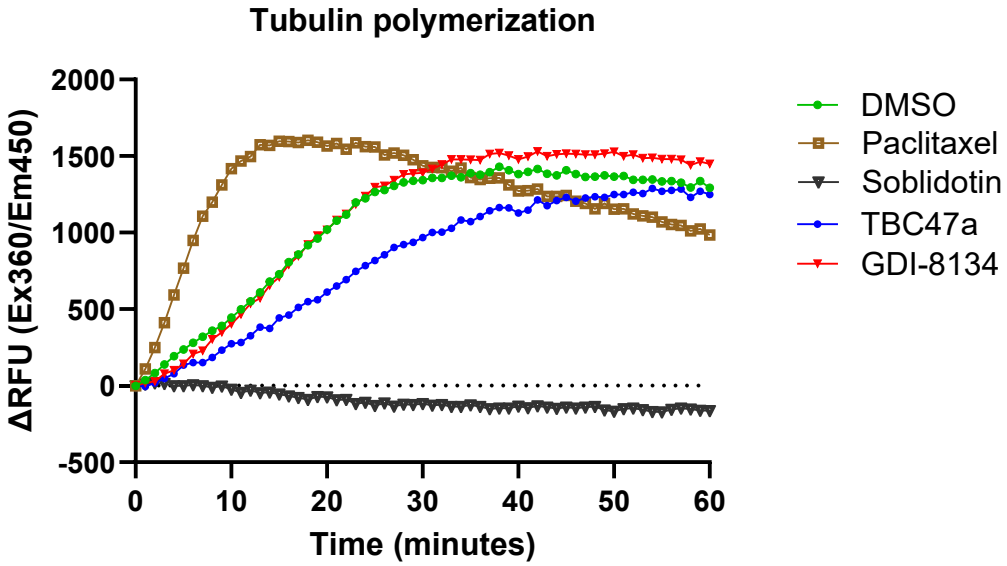
Supplementary Figure 5. Cytotoxicity of SB-RA-2001 in Vero E6 cells. Cell viability was measured after exposure to SB-RA-2001 in tissue-culture medium. The concentration-dependent decrease in viability plateaued at approximately 10 μM, likely because of the compound's poor solubility.



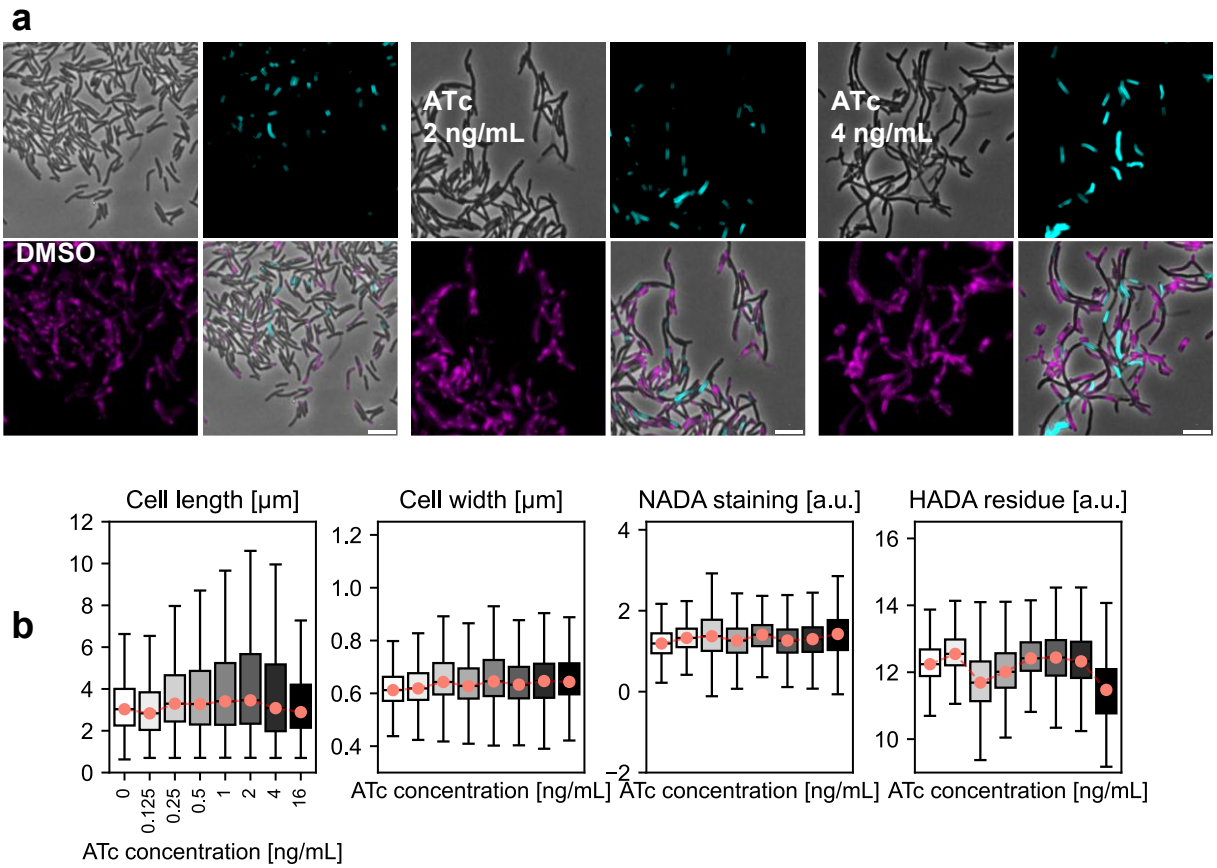
Supplementary Figure 6. Dynamic light-scattering analysis of MtbFtsZ polymerization and depolymerization. (**a**) MtbFtsZ polymerization was monitored after GTP addition. Each reaction contained 4 μM purified MtbFtsZ in buffer containing 50 mM MES (pH 6.5), 100 mM KCl, and 5 mM $MgCl_2$. Measurements were initiated immediately after adding GTP and collected at 25°C using a Wyatt DynaPro Plate Reader III (Waters) equipped with an 830-nm laser. The mean hydrodynamic radius (r_h) of MtbFtsZ assemblies was calculated using DYNAMICS 8.3 software, and polymerization profiles were plotted as the radius versus time using GraphPad Prism 11. (**b, c**) Effects of SS-18 and GDI-B029 on MtbFtsZ polymerization were monitored by DLS. Both compounds are sulindac sulfide derivatives that bind MtbFtsZ (see main text, Table 1, and Supplementary Fig. 4). Reactions contained the same buffer and MtbFtsZ concentration described above. Test compounds were added at 50 μM, with DMSO as the vehicle control. Samples were centrifuged before measurement to remove insoluble material. Polymerization was initiated by adding GTP to 60 μM. Data acquisition and analysis were performed as described for panel **a**. Experiments were performed twice on separate days; representative traces are shown.



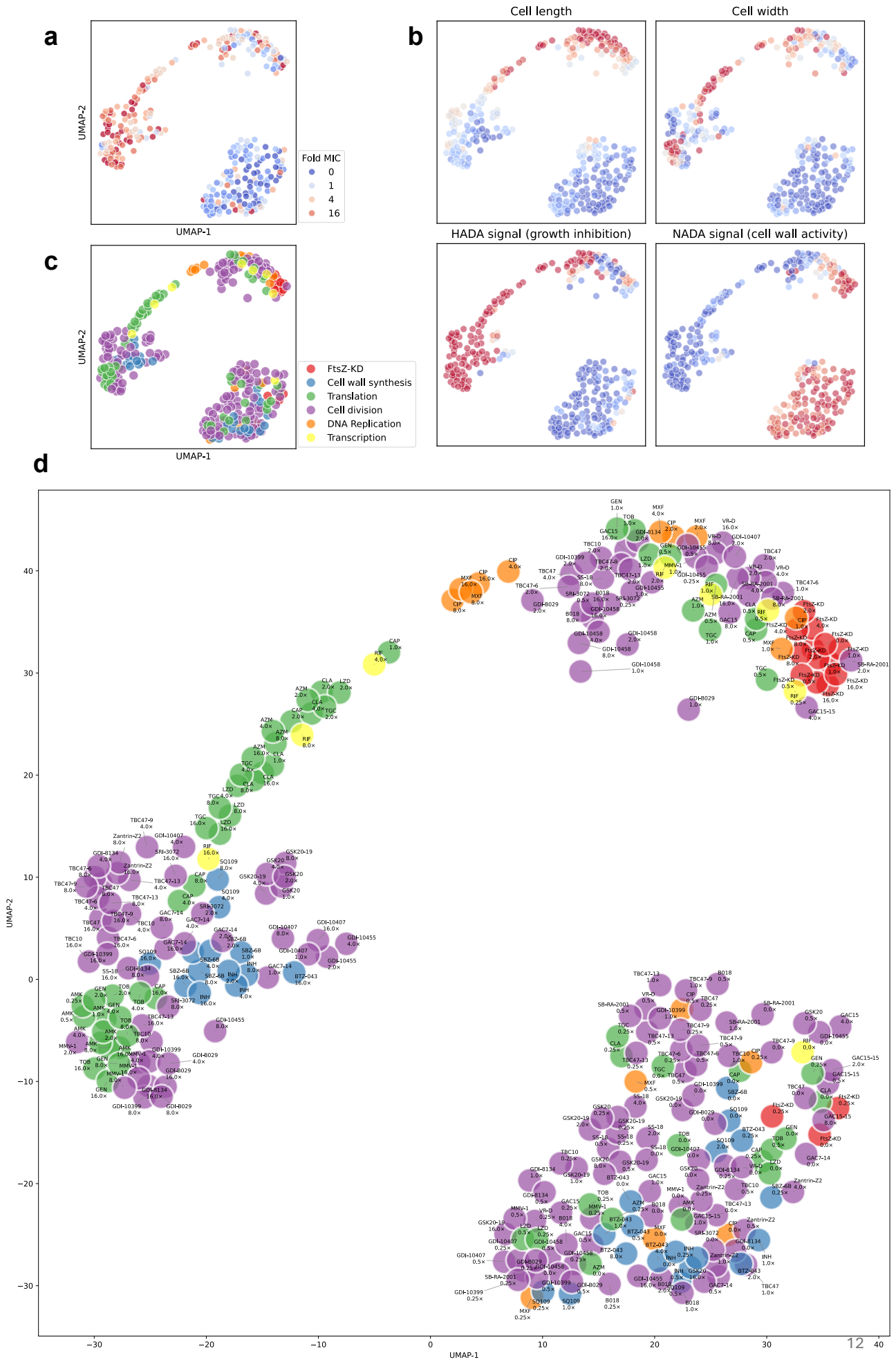
Supplementary Figure 7. Biological validation of TBC47 compounds as MtbFtsZ inhibitors. (**a**) Key primary-assay results for resupplied TBC47 compounds. Shaded regions in TBC47a indicate the structural modifications represented among the commercially available analogs. (**b**) Average cell length and representative images of wild-type BCG cells treated with TBC47 compounds. (**c**) MIC50-shift assay in the *ftsZ*-KD strain GH161, supporting cellular target engagement by the TBC47 compounds. (**d**) DLS analysis of TBC47 compounds at 50 µM, a concentration near their enzymatic IC50 values. TBC47a completely inhibited MtbFtsZ polymerization, whereas TBC47c delayed depolymerization. Experiments were performed in triplicate, and representative records are shown.



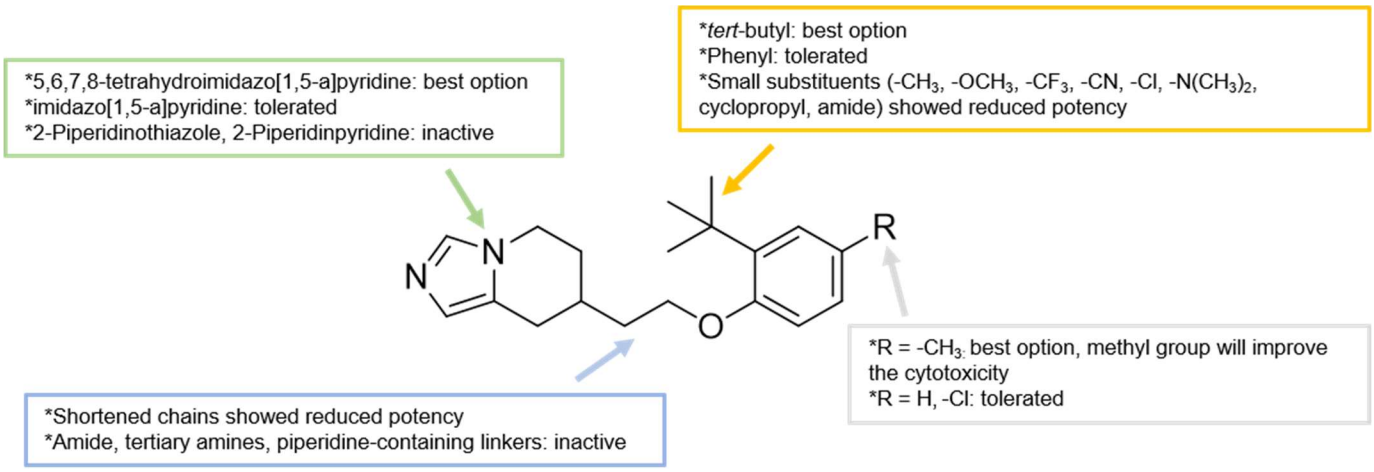
Supplementary Figure 8. Tubulin polymerization assay with selected MtbFtsZ screening hits. Tubulin polymerization was measured using a commercial assay kit (Cytoskeleton, Inc.) according to the manufacturer's instructions. Reactions contained 2 mg/mL (~18 μM) porcine tubulin in buffer comprising 80 mM PIPES (pH 6.9), 0.5 mM EGTA, and 2.0 mM $MgCl_2$. Polymerization was initiated with 1 mM GTP and approximately 7 μM DAPI fluorescence reagent and monitored at 37°C using a plate reader. Paclitaxel (4 μM) and soblidotin (100 μM) were included as positive controls for tubulin polymerization and inhibition, respectively. TBC47a and GDI-8134 were tested at 100 μM, with DMSO as the vehicle control. Compounds were dispensed into 20-μL reactions using an Echo liquid handler. ΔRFU = $RFU_{initial}$ - $RFU_{background}$.

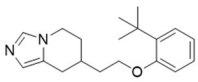
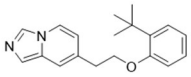
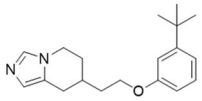
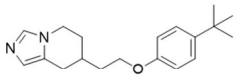
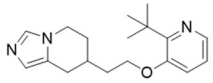
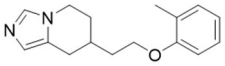
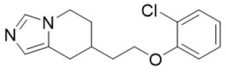
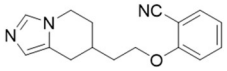
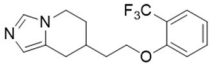
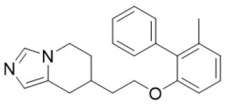
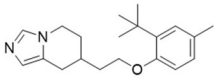
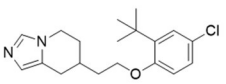


Supplementary Figure 9. CRISPRi-mediated genetic depletion of FtsZ phenocopies chemical inhibition of FtsZ. (**a**) Representative micrographs of BCG strain GH161 carrying the ATc-inducible CRISPRi construct targeting *ftsZ*, treated with DMSO or ATc at the indicated concentrations for 96 h. Phase-contrast, NADA (cyan; de novo peptidoglycan insertion), HADA (magenta; pre-existing cell-wall label), and merged channels are shown (scale bars, 5 µm). (**b**) Single-cell quantification of cell length, cell width, NADA staining intensity, and HADA residue intensity across an ATc titration series (0–16 ng/mL). Box plots show median and interquartile range; red dots indicate condition means (n ≥ 100 cells per condition). Partial FtsZ depletion induces progressive cell elongation with maximal filamentation at 1–2 ng/mL ATc, whereas the highest dose (16 ng/mL) yields shorter cells, consistent with severe growth arrest. Cell width and NADA staining remain essentially unchanged across the titration, indicating that cell-wall synthesis persists despite division arrest—a phenotype distinct from cell-wall synthesis inhibitors.

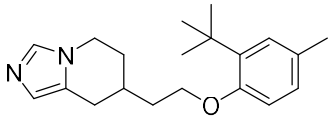

a
UMAP-2
UMAP-1
Fold MIC
0
1
4
16
b
Cell length
Cell width
HADA signal (growth inhibition)
NADA signal (cell wall activity)
c
UMAP-2
UMAP-1
FtsZ-KD
Cell wall synthesis
Translation
Cell division
DNA Replication
Transcription
d
UMAP-2
UMAP-1

Supplementary Figure 10. UMAP embedding of cytological profiles resolves dose-dependent trajectories and mechanism-specific clusters. (**a**) UMAP projection of all sample-level cytological profiles, colored by treatment dose (fold MIC; blue, 0×; light blue, 1×; light red, 4×; red, 16×). Vehicle and low-dose samples converge on a shared region, whereas increasing doses drive samples outward along mechanism-specific trajectories. (**b**) The same UMAP embedding overlaid with mean single-cell features: cell length, cell width, HADA residue signal (growth inhibition), and NADA signal (cell-wall synthesis activity). Feature values are Z-scored and shown on a blue–red scale. (**c**) UMAP embedding colored by mechanism of action: FtsZ knockdown (red), cell-wall synthesis inhibitors (blue), translation inhibitors (green), cell-division inhibitors (purple), DNA-replication inhibitors (orange), and transcription inhibitors (yellow). (**d**) Magnified view of (**c**), with each sample annotated as compound–fold MIC (e.g., RIF-16×, TBC47-1×). Point color denotes mechanism class as in (**c**); dashed trajectories connect increasing doses of individual compounds. FtsZ inhibitor hits (purple) co-cluster with the genetic FtsZ knockdown (red) at high dose, supporting on-target FtsZ inhibition.



GDI-ID	Structure	TSA ΔTm (℃)	GTPase IC50 (μM)	Mtb MIC (μM)	Vero, CC50 (μM)
GDI-8434		-1.7	53	5.7	32
GDI-8435		-0.7	30	8.5	33
GDI-9253		-0.5	66	14	31
GDI-8837		-1.4	52	11	25
GDI-9290		-0.1	33	65	86
GDI-9197		-0.4	>100	46	90
GDI-9198		-0.4	>100	47	80
GDI-9225		-0.2	>100	>100	>100
GDI-9226		-0.6	68	65	65
GDI-9474		-1.8	19	6.2	/
GDI-8838		-3.7	24	4.4	45
GDI-8937		-5.7	14	6.0	24

Supplementary Figure 11. Optimization and structure–activity relationship of GDI-8434 series. The screening hit GDI-8134 contained a potentially metabolically labile linear linker. Cyclization of this linker while preserving the overall chain length yielded GDI-8434. Positional scanning of the tert-butyl substituent on the right-hand phenyl ring, using GDI-8434, GDI-9253, and GDI-8837, showed that ortho substitution improved both thermal-shift and antibacterial activity. Replacing the tert-butyl group with methyl, chloro, cyano, trifluoromethyl, or cyclopropyl substituents did not improve either ΔT_m or MIC relative to GDI-8434, suggesting that the right-hand phenyl ring occupies a hydrophobic pocket. The designed analog GDI-9474 did not improve TSA or whole-cell activity. Although *meta*-chloro disubstitution increased ΔT_m, this effect did not translate into improved MIC values. GDI-8838 showed similar potency to GDI-8434 but lower cytotoxicity, resulting in an approximately twofold increase in the selectivity index from ~5 to ~10. GDI-8937 inhibited MtbFtsZ GTPase activity with an IC50 of ~14 μM, but did not improve antibacterial activity and showed increased cytotoxicity.



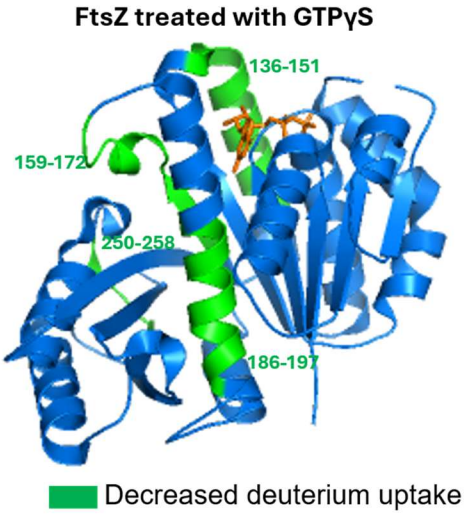
GDI-8838

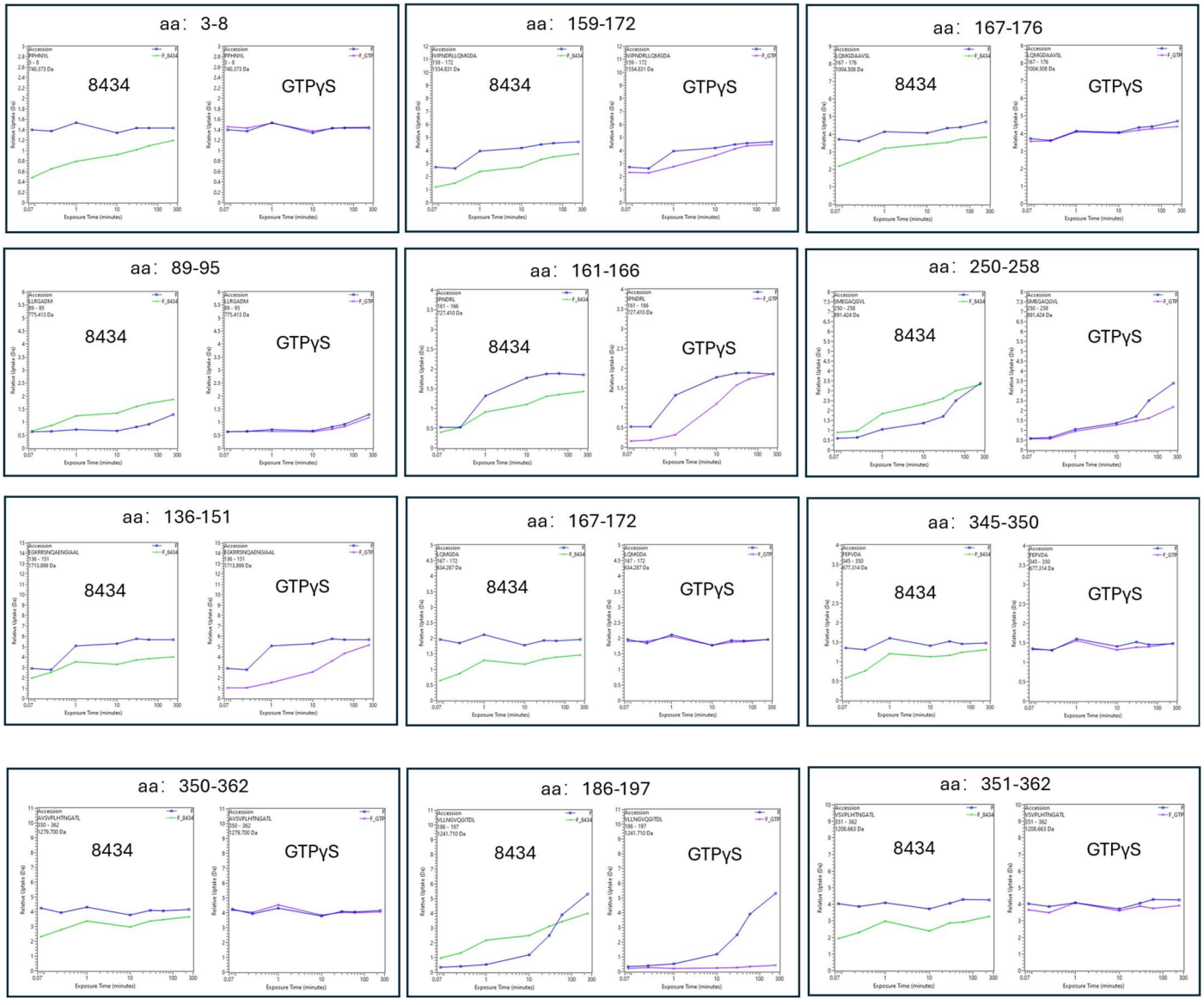
Molecular weight/cLogP: 312/5.0
Mtb MIC (μM): 4.4
Rat microsomal CL (μL/min/mg): 13.8
Human microsomal CL (μL/min/mg): 13.7
Rat plasma protein binding (%): 99.6%
Human plasma protein binding (%): 99.7%
Solubility (pH 6.8, μM): 96.8

Supplementary Figure 12. Tier 1 DMPK data of GDI-8838.

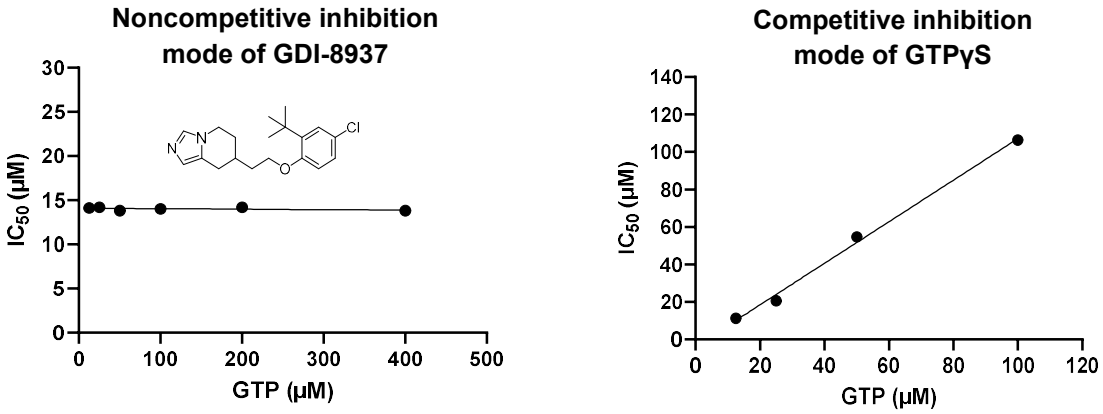
a

Aa	Sequence	Deuterium uptake (8434)	Deuterium uptake (GTPγS)
3-8	PPHNYL	Decreased	unchanged
89-95	LLRGADM	Increased	unchanged
136-151	EGKRRSNQAENGIAAL	Decreased	Decreased
159-172	IVIPNDRLLQMGDA	Decreased	Decreased
161-166	IPNDRL	Decreased	Decreased
167-172	LQMGDA	Decreased	unchanged
167-176	LQMGDAAVSL	Decreased	unchanged
186-197	VLLNGVQGITDL	Increased	Decreased
250-258	SMEGAQGVL	Increased	Decreased
345-350	FEPVDA	Decreased	unchanged
350-362	AVSVPLHTNGATL	Decreased	unchanged
351-362	VSVPLHTNGATL	Decreased	unchanged

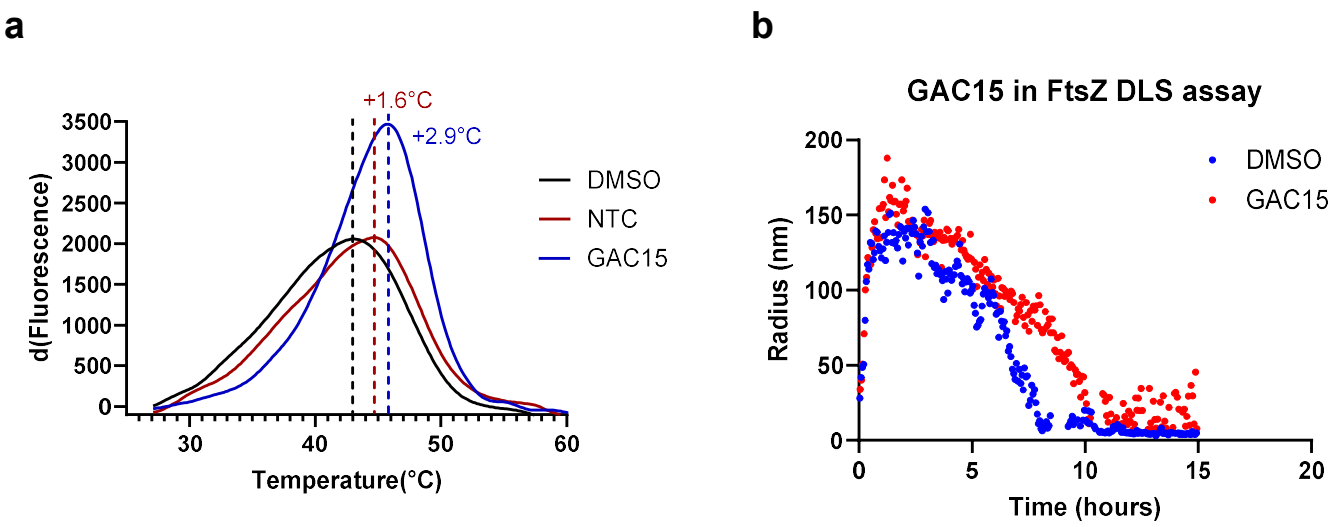




b

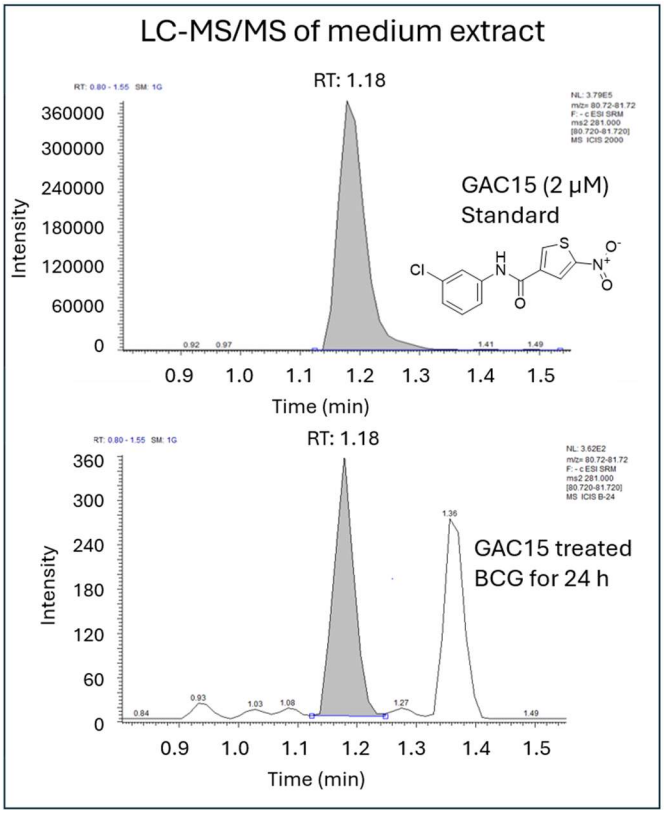


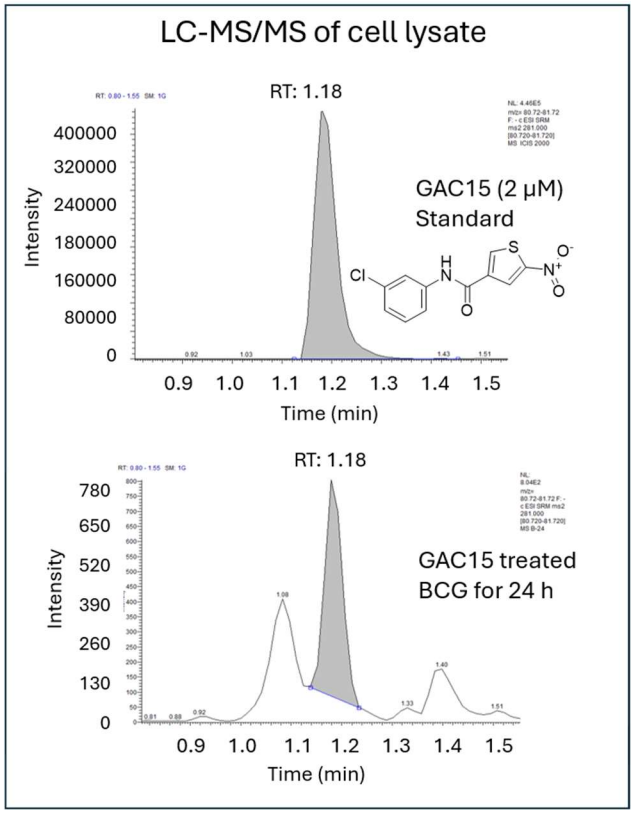
Supplementary Figure 13. Mode-of-action analysis of GDI-8434 series against MtbFtsZ. (**a**) Time-resolved HDX-MS profiles of selected MtbFtsZ peptides. The peptides with altered deuterium uptake upon treatment of MtbFtsZ with GDI-8434 or GTPγS are summarized in a table. The peptides with decreased deuterium uptake upon GTPγS treatment are mapped onto the structures for comparison with GDI-8434 treatment (Figure 4D). In the lower portion, each panel shows deuterium uptake for one peptide, identified by its residue range, following treatment with the allosteric modulator GDI-8434 or the orthosteric ligand GTPγS. The y-axis indicates relative deuterium incorporation (Da), and the x-axis indicates deuterium-exposure time on a logarithmic scale. The uptake differences reflect ligand-dependent changes in solvent accessibility and local conformational dynamics. (**b**) GDI-8937 inhibited MtbFtsZ GTPase activity in a manner consistent with noncompetitive inhibition with respect to GTP, whereas GTPγS competed with GTP for binding at the active site.



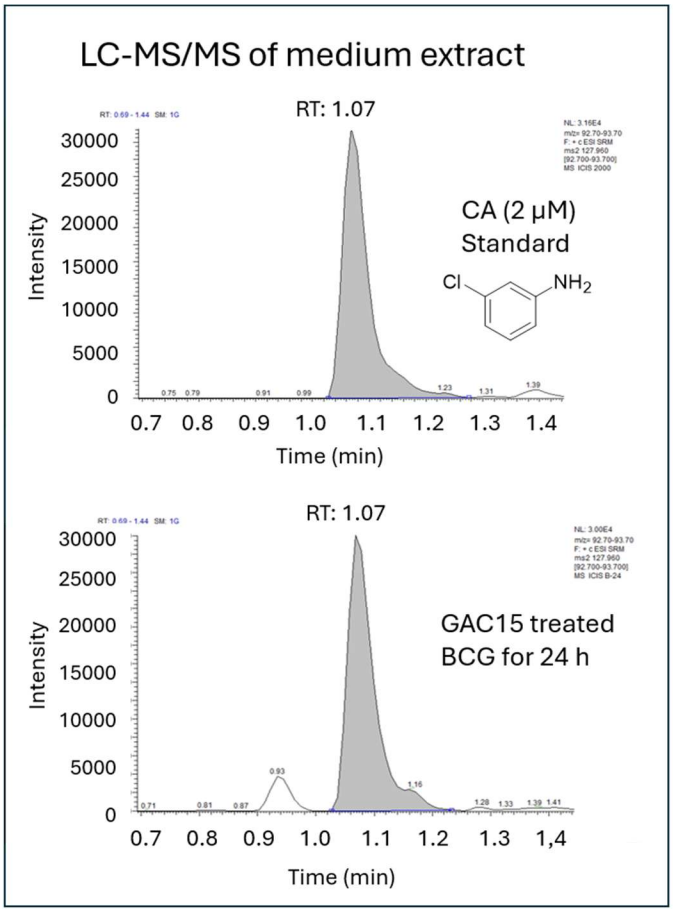
Supplementary Figure 14. FtsZ assays demonstrated that GAC15 and its derivatives inhibit MtbFtsZ in vitro. (**a**) Thermal shift assay of MtbFtsZ in the presence of 50 μM of each compound, shown as the first derivative of dye-based DSF (differential scanning fluorimetry). (**b**) Dynamic light scattering of MtbFtsZ polymerization and depolymerization in the presence of 50 μM GAC15, recorded on a DynaPro Plate Reader III.

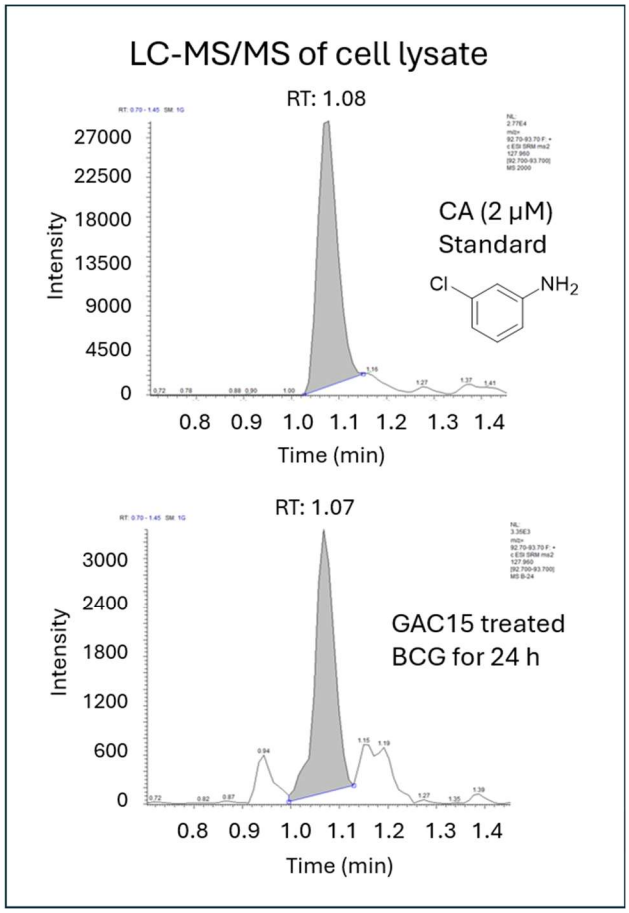
a


LC-MS/MS of medium extract
RT: 1.18
GAC15 (2 μM)
Standard
Intensity
Time (min)
RT: 1.18
GAC15 treated
BCG for 24 h
Intensity
Time (min)

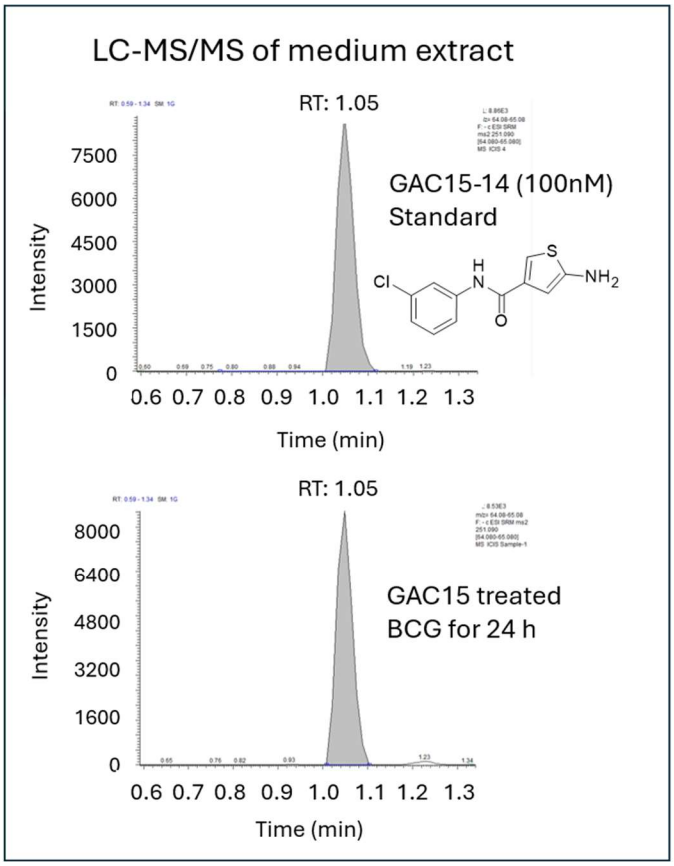

LC-MS/MS of cell lysate
RT: 1.18
GAC15 (2 μM)
Standard
Intensity
Time (min)
RT: 1.18
GAC15 treated
BCG for 24 h
Intensity
Time (min)

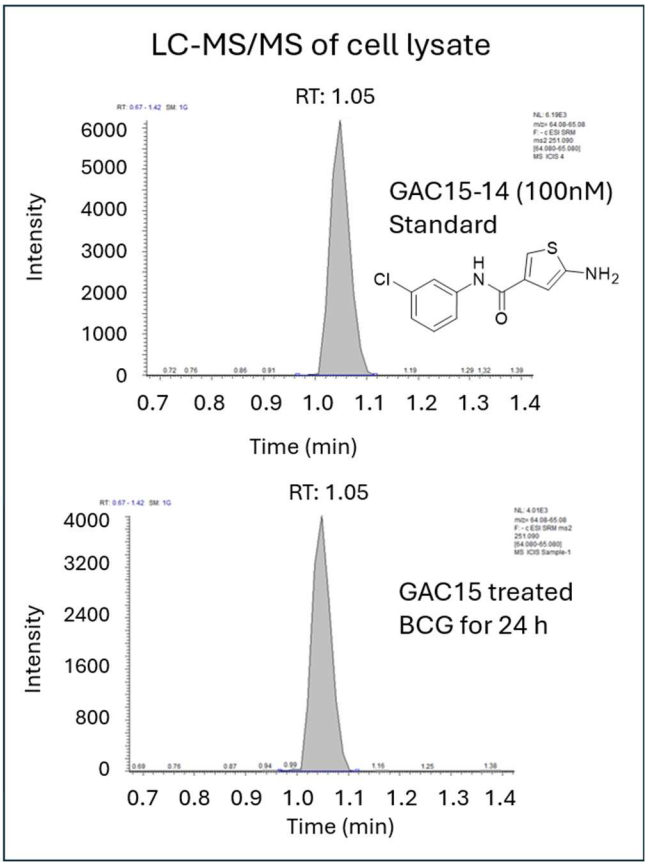
b


LC-MS/MS of medium extract
RT: 1.07
CA (2 μM)
Standard
Intensity
Time (min)
RT: 1.07
GAC15 treated
BCG for 24 h
Intensity
Time (min)

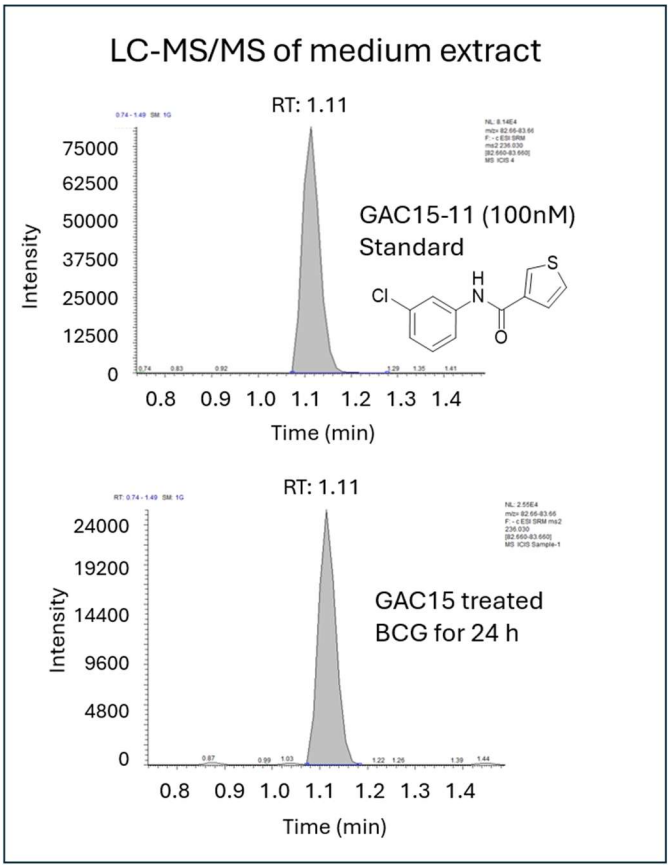

LC-MS/MS of cell lysate
RT: 1.08
CA (2 μM)
Standard
Intensity
Time (min)
RT: 1.07
GAC15 treated
BCG for 24 h
Intensity
Time (min)

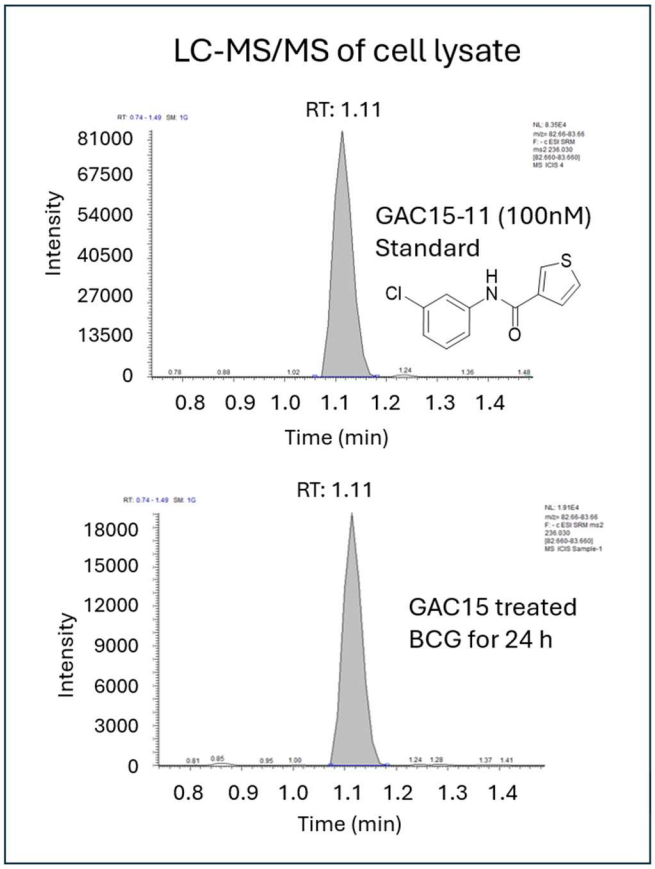
c


LC-MS/MS of medium extract
RT: 1.05
GAC15-14 (100nM)
Standard
Intensity
Time (min)
RT: 1.05
GAC15 treated
BCG for 24 h
Intensity
Time (min)


LC-MS/MS of cell lysate
RT: 1.05
GAC15-14 (100nM)
Standard
Intensity
Time (min)
RT: 1.05
GAC15 treated
BCG for 24 h
Intensity
Time (min)

d


LC-MS/MS of medium extract
RT: 1.11
GAC15-11 (100nM)
Standard
Intensity
Time (min)
RT: 1.11
GAC15 treated
BCG for 24 h
Intensity
Time (min)


LC-MS/MS of cell lysate
RT: 1.11
GAC15-11 (100nM)
Standard
Intensity
Time (min)
RT: 1.11
GAC15 treated
BCG for 24 h
Intensity
Time (min)

Supplementary Figure 15. LC–MS/MS multiple-reaction monitoring (MRM) analysis of GAC15 metabolites in *M. bovis* BCG cultures. Exponentially growing BCG cultures were treated with 20 μM GAC15 for 24 h. Extracts from the culture medium and cell lysates were analyzed by targeted LC–MS/MS using multiple-reaction monitoring. (**a**) GAC15 detected under negative-ionization conditions. (**b**) *m*-Chloroaniline (CA) detected under positive-ionization conditions. (**c**) GAC15-14 detected under negative-ionization conditions. (**d**) GAC15-11 detected under negative-ionization conditions. Experimental procedures are described in the Methods.

Supplementary Table 1. Identity and similarity of FtsZ protein sequences deduced from the genomes of *Mycobacterium* species and compared to that of *Mtb* H37Rv.

Mycobac spp. vs. Mtb H37Rv	***Mtb H37Ra***	***M. bovis***	***M. leprae***	***M. avium***	***M. kansasii***	***M. xenopi***	***M. malmoense***	***M. simiae***
FtsZ identity	100%	100%	96.6%	95.3%	89.4%	91.9%	95.6%	96.1%
FtsZ similarity	/	/	97.9%	97.2%	93.5%	93.7%	97.9%	97.2%

Supplementary Table 2. Key data for synthesized analogs of primary screening hits shown in Fig. 2c. Data for the remaining compounds are provided in Table 1. GAC7-14 and VR-D (purchased Dacomitinib) are screening hits that have not yet been confirmed by resynthesis.

Compound ID	TSA ΔTm (℃)[1]	GTPase inh (%)[2]	MIC50 shift* (ATc=0/ATc=2)[3]	BCG cell Δlength (μm)[4]	Mtb H37Rv MIC (μM)[3]	Vero 6 CC50 (μM)
TBC47b	-1.7 ± 0.1	93 ± 5	3.7	1.2	5.0	5.8
TBC47c	-2.1 ± 0.2	79 ± 3	2.2	1.0	2.8	3.3
TBC47d	-1.8 ± 0.4	100 ± 6	3.6	1.3	6.2	10.6
GDI-10399-1	-2.5 ± 0.2	100 ± 10	3.0	1.3	4.1	8.3
GDI-B018	-1.7 ± 0.2	65 ± 2	1.7	1.9	28.1	22.5
GDI-B029	-1.1 ± 0.3	76 ± 8	1.6	0.7	10.8	5.1
VR-D	0.8 ± 0.1	4 ± 5	1.2	0.4	24.9	>100
GAC7-14	1.7 ± 0.3	1 ± 3	1.5	0.4	>100	>100
GSK20b	1.1 ± 0.1	0 ± 1	2.5	1.1	78.1	>100
GDI-10455-1	4.8 ± 0.3	89 ± 9	1.8	0.9	45.5	11.8

[1] Compound at 50 μM; n=3, mean ± SD.
[2] 16-hour pre-incubation with compound at 100 μM; n=3, mean ± SD.
[3] Microbiological measures were performed at least twice. A representative value or average is shown.
[4] Difference of average cell lengths between treatments of a compound at 1x MIC and DMSO for about 100 wild-type cells.
* A value of MIC50 shift means the fold difference in MIC50 when the inducer ATc is absent versus present at 2 ng/mL.

Supplementary Table 3. MIC values for GAC15 and pretomanid against wild-type BCG and GAC15-resistant mutants. MICs were determined for GAC15 and pretomanid (Pa) against wild-type BCG (WT) and the GAC15-resistant mutant strains (M).

	WT	**M1**	**M2**	**M3**	**M4**	**M6**	**M9**
GAC15 (μM)	1.5	83	102	76	81	58	93
Pa (μM)	0.030	0.031	0.034	0.034	0.024	0.033	0.025

Supplementary Table 4. Bacterial strains and plasmids used in this study.

Strains	Description	Reference or source
M. bovis	*Mycobacterium bovis* (strain BCG/ Pasteur 1173P2)	L. Lyu in Fudan University
GH161	*M. bovis* BCG derivative; BCG was transformed with the pLJR965 expressing the sgRNA to target the ftsZ gene	This study
DH5a	F- endA1 glnV44 thi-1 recA1 relA1 gyrA96 deoR nupG φ80lacZΔM15 Δ (lacZYA-argF) U169 hsdR17 (rK^- mK^+) λ^-	TransGen Biotech
BL21	F-dcm ompT hsdS(r_B- m_B-) gal [$malB^+$]$_{K-12}$(λ^S)	TransGen Biotech
Plasmids		
pLJR965	Sth1 dCas9 TetR and KanR L5 Int attP for *M. tuberculosis*	Addgene #115163
pET28a	*E. coli* protein expression vector, Kan^r	Novagen

Supplementary Table 5. Primers for analysis of the CRISPRi *ftsZ*-KD strain by PCR or qRT-PCR.

Primers	Description	Gene or DNA	Reference or source
Pr2050	5-CACCAACTGGTCCACCTAC-3	pJLR965 verification	This study
Pr2051	5-CCTGCGTTATCCCCTGAT-3		This study
Pr2276	TTGCTGCAGATGGGAGATG	*ftsZ*	This study
Pr2277	GTGGTAATCAGGTCGGTGATG		This study
pr2280	CAGCGATGGCCGATGAG	*pgeF*	This study
pr2281	CGACGTCGATAGACTCAACAC		This study
pr2282	CGGTGGTGGTCAAGGATTT	*ftsQ*	This study
pr2283	ATCGCTAGGACCGGGATT		This study
pr2284	CGGTCGCTATAAGGTCAACAA	*rpoB*	This study
pr2285	TGCAAGCGGACCAGATATTC		This study

Supplementary References

(1) Mathew, B.; Hobrath, J. V.; Ross, L.; Connelly, M. C.; Lofton, H.; Rajagopalan, M.; Guy, R. K.; Reynolds, R. C. Screening and Development of New Inhibitors of FtsZ from M. Tuberculosis. *PLOS ONE* **2016**, *11* (10), e0164100. https://doi.org/10.1371/journal.pone.0164100.

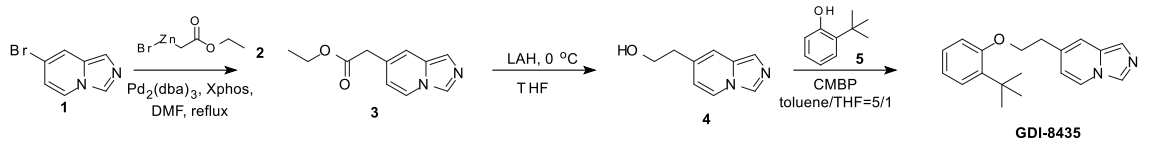
(2) Gao, K.; Oerlemans, R.; Groves, M. R. Theory and Applications of Differential Scanning Fluorimetry in Early-Stage Drug Discovery. *Biophys. Rev.* **2020**, *12* (1), 85–104. https://doi.org/10.1007/s12551-020-00619-2.

(3) Llowarch, P.; Usselmann, L.; Ivanov, D.; Holdgate, G. A. Thermal Unfolding Methods in Drug Discovery. *Biophys. Rev.* **2023**, *4* (2), 021305. https://doi.org/10.1063/5.0144141.

(4) Huynh, K.; Partch, C. L. Analysis of Protein Stability and Ligand Interactions by Thermal Shift Assay. *Curr. Protoc. Protein Sci.* **2015**, *79* (1). https://doi.org/10.1002/0471140864.ps2809s79.

Synthetic chemistry methods

GDI-8435

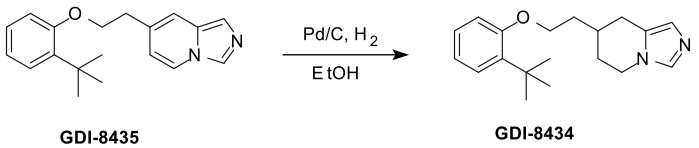


Synthesis of compound **3**: Add chlorotrimethylsilane (0.233 g, 2.10 mmol) to a mixture of zinc (2.55 g, 39.0 mmol) in tetrahydrofuran (20 mL) at 15 ºC. The mixture is stirred for 15 min and then a solution of ethyl bromoacetate (5.11 g, 30.0 mmol) in tetrahydrofuran (10 mL) is added dropwise. The reaction is heated to 40 ºC for 30 min. The mixture is cooled to 20 ºC and the supernatant liquid is used as title compound **2** (30 mmol, 1 mol/L, 100%) in the next step directly. Add compound **2** (10.2 mL, 10.2 mmol, 1 mol/L) to a mixture of compound **1** (400 mg, 2.04 mmol), $Pd_2(dba)_3$ (373 mg, 0.408 mmol,) and Xphos (384 mg, 0.816 mmol) in DMF (10 mL) under nitrogen. The reaction is heated to 70 ^{0}C for 2 hours. The reaction is quenched with saturated NH_4Cl solution (30 mL) and extracted with EtOAc (30 mL * 3). The combined organic layers are washed with brine (30 mL), dried over anhydrous sodium sulfate, filtered, and concentrated. The residue is purified by flash chromatography eluting with DCM/MeOH (10:1) to give compound **3** (200 mg, 48% yield) as a yellow solid, ESI-MS: $[M+H]^+$, 204.85.

Synthesis of compound **4**: To a solution of compound **3** (150 mg, 0.74 mmol) in THF (2 ml) stirred was added LAH (3.7 ml, 3.71 mmol, 1M in THF) dropwise at 0 ºC. The reaction mixture was stirred at rt for 1 hour. The mixture was quenched with 15% NaOH solution, dried over anhydrous sodium sulfate, filtered, and concentrated under vacuum to give compound **4** (100 mg, 85% yield) as a colorless oil, ESI-MS: $[M+H]^+$, 162.85.

Synthesis of compound **GDI-8435**: A round-bottom flask containing a mixture of **compound 4** (90 mg, 0.55 mmol), **compound 5** (84 mg, 0.55 mmol) and CMBP (398 mg, 1.65 mmol) with toluene/THF=5/1 (5 mL) under N_2 was placed at 100 ºC and stirred for 15 hours. The solution was filtered; filtrate was collected. The reaction mixture was concentrated under pressure at 60 ℃ and purified by prep-HPLC (column: Phenomenex luna C18 250 mm x 100 mm x 10 um; mobile phase: (H_2O (0.1% $NH3.H_2O$)-ACN); B%: 30% - 70%, 40 min) to give **GDI-8435** (80 mg, 46.53% yield) as a white solid, ESI-MS: $[M+H]^+$, 295.10. **^{1}H NMR** (400 MHz, MeOD) δ 9.24 (d, *J* = 11.5 Hz, 1 H), 8.43 (d, *J* = 7.1 Hz, 1 H), 7.83 (d, *J* = 6.3 Hz, 1 H), 7.71 (s, 1 H), 7.25 – 7.10 (m, 3 H), 6.97 (d, *J* = 8.3 Hz, 1 H), 6.84 (t, *J* = 7.5 Hz, 1 H), 4.36 (t, *J* = 6.1 Hz, 2 H), 3.22 (t, *J* = 5.9 Hz, 2 H), 1.24 (s, 9 H).

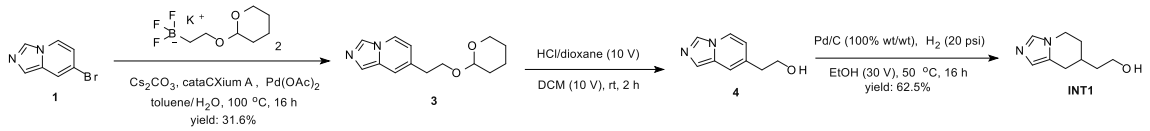
GDI-8434



Synthesis of compound **GDI-8434**: A round-bottom flask containing a mixture of **GDI-8435** (25 mg, 0.085 mmol), and Pd/C (56 mg, 0.425 mmol) with EtOH (3 mL) under H_2 was placed at 25ºC and stirred for 2 hours. The solution was filtered; and the mixture

was concentrated under pressure at 45 ℃ and purified by prep-HPLC (column number: Phenomenex luna C18 250 mm x 100 mm x 10 um; mobile phase: (H_2O (0.1% TFA)-ACN); B%: 30% - 70%, 40 min) to give **GDI-8434** (7.38 mg, 30% yield) as a colorless oil, ESI-MS: $[M+H]^+$, 299.30. **^{1}H NMR** (400 MHz, MeOD) δ 8.75 (s, 1 H), 7.31 – 7.21 (m, 2 H), 7.17 – 7.11 (m, 1 H), 6.97 (d, *J* = 7.8 Hz, 1 H), 6.90 – 6.81 (m, 1 H), 4.49 – 4.45 (m, 1 H), 4.21 – 4.11 (m, 3 H), 3.18 (dd, *J* = 16.4, 4.9 Hz, 1 H), 2.57 (dd, *J* = 16.0, 11.2 Hz, 1 H), 2.29 – 2.21 (m, 2 H), 2.09 – 1.96 (m, 2 H), 1.86 – 1.81 (m, 1 H), 1.38 (s, 9 H).

INT1 synthesis

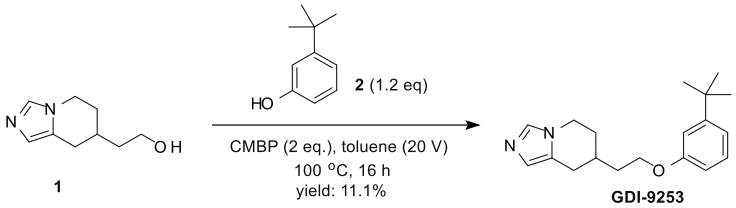


Synthesis of compound **3**: compound **1** (250 mg, 1.27 mmol, 1 eq) and compound **2** (359 mg, 1.52 mmol, 1.2 eq) were dissolved in toluene (5 mL) and H_2O (0.5 mL). Cs_2CO_3 (1.24 g, 3.81 mmol, 3 eq), CataCXium A (91.0 mg, 254 μmol, 0.2 eq), and $Pd(OAc)_2$ (28.5 mg, 127 μmol, 0.1 eq) were added sequentially at 20 °C. The reaction mixture was stirred at 100 °C for 16 hours under a nitrogen atmosphere, and reaction completion was confirmed by LCMS. H_2O (30 mL) was added to the mixture, and the aqueous phase was extracted with EtOAc (20 mL * 3). The combined organic phases were washed with saturated aqueous NaCl (20 mL), concentrated under reduced pressure, and purified by silica gel chromatography (SiO_2, EtOAc) to afford the target compound **3** (550 mg, 2.00 mmol, 31.6% yield) as a yellow oil, ESI-MS: $[M+H]^+$, 247.0.

Synthesis of compound **4**: compound **3** (500 mg, 2.03 μmol, 1 eq) was dissolved in DCM (5 mL), and 4 M HCl/dioxane (5 mL) was added at 20 °C. The reaction mixture was stirred at 25 °C for 2 hours, and reaction completion was confirmed by LCMS. The mixture was concentrated under reduced pressure, and H_2O (5 mL) was added. The pH of the aqueous phase was adjusted to approximately 7 using saturated aqueous $NaHCO_3$ (1 mL), followed by extraction with EtOAc (3 mL * 3). The combined organic layers were washed with saturated aqueous NaCl (5 mL) and concentrated under reduced pressure to yield the target compound **4** (310 mg, crude) as a yellow oil, ESI-MS: $[M+H]^+$, 162.9.

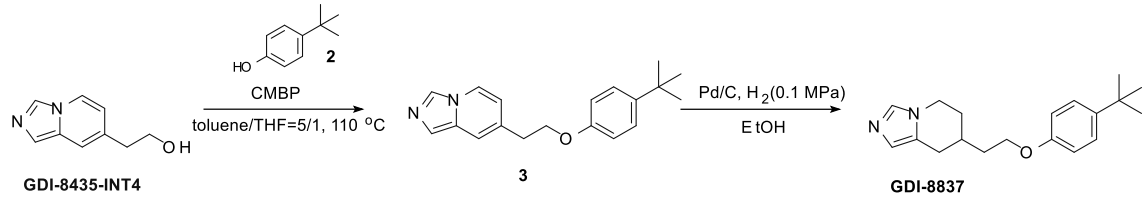
Synthesis of **INT1**: Under an argon atmosphere, Pd/C (250 mg, 10% purity) was added to a reaction flask, followed by the slow addition of EtOH (7.5 mL) to completely wet Pd/C. Compound **4** (250 mg, 1.54 mmol, 1 eq) was added at 20 °C. The reaction mixture was stirred at 50 °C under a hydrogen atmosphere (20 psi) for 16 hours; and reaction completion was confirmed by LCMS. The reaction mixture was filtered through Celite, and the filter cake was washed with EtOH (100 mL). The combined organic phases were concentrated under reduced pressure to yield the target **INT1** (200 mg, 964 μmol, 62.5% yield) as a yellow oil, ESI-MS: $[M+H]^+$, 167.0.

GDI-9253



Synthesis of compound **GDI-9253**: compound **INT1** (50 mg, 301 μmol, 1 eq) and compound **2** (54.2 mg, 361 μmol, 1.2 eq) were dissolved in toluene (1 mL), and CMBP (145 mg, 606 μmol, 2 eq) was added at 25 °C. The reaction mixture was stirred at 100 °C for 16 hours under a nitrogen atmosphere, and reaction completion was confirmed by LCMS. The mixture was concentrated under reduced pressure and purified via silica gel chromatography (SiO_2, EtOAc/MeOH = 10/1) followed by high-performance liquid chromatography (column: WePure Biotech XP tC18 150×40 mm, 70 μm; mobile phase: [H2O (10 mM NH4HCO3)–ACN]; gradient: 20%–50% B over 8.0 min) to afford the target compound **GDI-9253** (10 mg, 33.5 μmol, 11.1% yield, 100% purity) as a yellow oil, ESI-MS: $[M+H]^+$, 299.2. **^{1}H NMR** (400 MHz, Chloroform-d_3) δ = 7.50 (s, 1 H), 7.24 (t, *J* = 8.0 Hz, 1 H), 7.04 - 6.98 (m, 1 H), 6.94 (t, *J* = 2.1 Hz, 1 H), 6.78 (s, 1 H), 6.72 (td, *J* = 1.2, 8.1 Hz, 1 H), 4.27 - 4.16 (m, 1 H), 4.09 (dt, *J* = 2.1, 6.1 Hz, 2 H), 3.94 (dt, *J* = 4.6, 11.9 Hz, 1 H), 3.06 (dd, *J* = 5.1, 15.7 Hz, 1 H), 2.43 (dd, *J* = 11.0, 15.6 Hz, 1 H), 2.23 - 2.10 (m, 2 H), 1.92 - 1.82 (m, 2 H), 1.80 - 1.69 (m, 1 H), 1.32 (s, 9 H).

GDI-8837

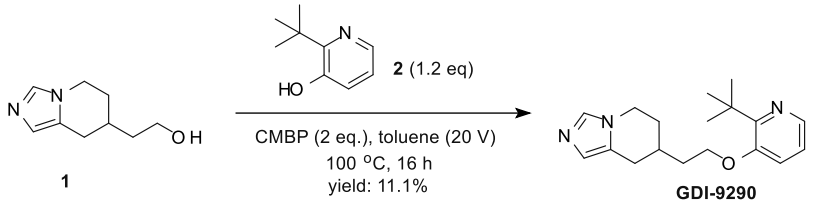


Synthesis of compound **3**: A solution of **GDI-8435-INT4** (100 mg, 0.62 mmol), 4-tert-butylphenol (139 mg, 0.92 mmol) and CMBP (298 mg, 1.23 mmol) in toluene (5 mL) stirred under nitrogen at 100°C for 16 h. LCMS showed starting material was consumed and desired mass was observed. After that the solution was poured into H_2O (20 mL). The solution was extracted with EtOAc (20 mL*3) and dried over Na_2SO_4, filtered and concentrated to give a residue. The residue was purified by trituration with DCM:MeOH (50v:1v to 20v:1v) to give the pure compound **3** (80 mg,0.27 mmol,44.06 % yield) as a yellow solid, ESI-MS: $[M+H]^+$, 295.10.

Synthesis of compound **GDI-8837**: A mixture of compound **3** (80 mg, 0.27 mmol) and Pd/C (14.5 mg, 0.14 mmol) in EtOH (5 mL) was stirred at 25°C for 16 hours under an atmosphere of H_2. After the mixture was filtered through celite and the filtrate was concentrated under vacuum. Then the reaction mixture was concentrated in vacuo, the residue was further purified by prep-HPLC (Gemini 5 um C18 column, 150*21.2 mm, eluting with 10% to 20% ACN/H_2O containing) to give the **GDI-8837** (42.54 mg, 0.14 mmol, 52.45% yield) as a yellow solid, ESI-MS: $[M+H]^+$, 298.80. **^{1}H NMR** (400 MHz, DMSO) δ 7.45 (s, 1 H), 7.27 (m, 2 H), 6.86 (m, 2 H), 6.58 (s, 1 H), 4.15 (m, 1 H), 4.05 (t,

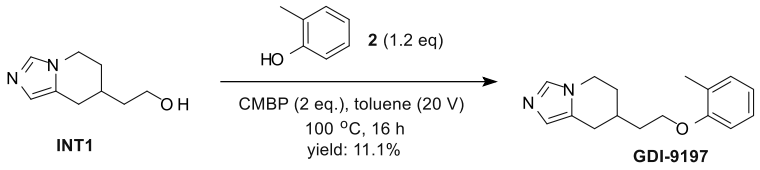
J = 6.4 Hz, 2 H), 3.84 (m 1 H), 2.93 (m, 1 H), 2.32 (m, 1 H), 2.01 (m, 2 H), 1.80 (m, 2 H), 1.61 (m, 1 H), 1.25 (s, 9 H).

GDI-9290



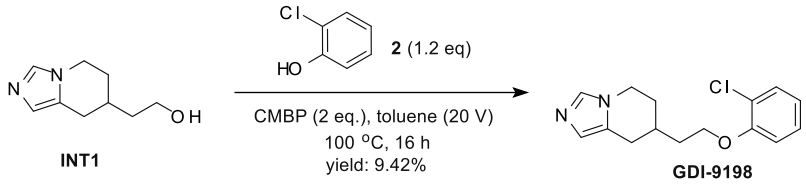
Synthesis of compound **GDI-9290**: compound **INT1** (40 mg, 241 μmol, 1 eq) and compound **2** (36.4 mg, 241 μmol, 1 eq) were dissolved in toluene (1 mL), and CMBP (116 mg, 481 μmol, 2 eq) were added at 25 °C. The reaction mixture was stirred at 100 °C for 16 hours under a nitrogen atmosphere, and reaction completion was confirmed by LCMS. The reaction mixture was concentrated under reduced pressure and purified sequentially via silica gel chromatography (SiO_2, EtOAc/Methanol = 10/1) and high-performance liquid chromatography (column: Waters Xbridge BEH C18 100 × 25 mm, 10 μm; mobile phase: [H_2O (10 mM NH_4HCO_3) – ACN]; gradient: 40%–70% B over 8.0 min) to afford the target compound **GDI-9290** (2 mg, 6.68 μmol, 2.78% yield) as a yellow oil, ESI-MS: $[M+H]^+$, 300.2. **^{1}H NMR** (400 MHz, DMSO-d_6) δ = 8.04 (dd, *J* = 1.3, 4.6 Hz, 1 H), 7.59 - 7.42 (m, 1 H), 7.40 (dd, *J* = 1.1, 8.3 Hz, 1 H), 7.21 (dd, *J* = 4.6, 8.3 Hz, 1 H), 6.74 - 6.49 (m, 1 H), 4.23 - 4.15 (m, 1 H), 4.15 - 4.11 (m, 2 H), 3.88 - 3.77 (m, 1 H), 2.96 (dd, *J* = 4.2, 15.3 Hz, 1 H), 2.41 - 2.34 (m, 1 H), 2.11 - 2.01 (m, 2 H), 1.95 - 1.86 (m, 2 H), 1.69 - 1.60 (m, 1 H), 1.35 (s, 9 H)

GDI-9197



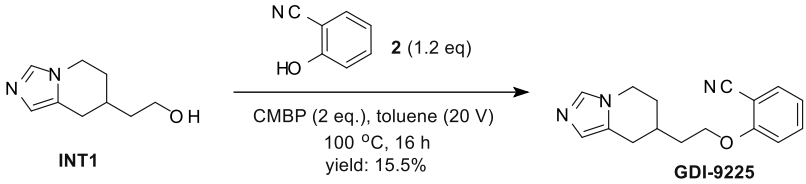
Synthesis of compound **GDI-9197**: compound **INT1** (50 mg, 241 μmol, 1 eq) and compound **2** (31 mg, 289 μmol, 1.2 eq) were dissolved in toluene (1 mL). CMBP (116 mg, 481 μmol, 2 eq) was added at 25 °C, and the reaction mixture was stirred at 100 °C for 16 hours under a nitrogen atmosphere, and reaction completion was confirmed by LCMS. The reaction mixture was concentrated under reduced pressure and purified via silica gel chromatography (SiO_2, EtOAc/MeOH = 10/1) followed by preparative HPLC (column: Waters Xbridge BEH C18 100 × 30 mm, 10 μm; mobile phase: [H_2O (10 mM NH_4HCO_3)–ACN]; gradient: 38%–68% B over 8.0 min) to afford the target compound **GDI-9197** (4.8 mg, 18.0 μmol, 7.47% yield, 96.0% purity) as a white solid, ESI-MS: $[M+H]^+$, 257.2. **^{1}H NMR** (400 MHz, Chloroform-d_3) δ = 7.41 (s, 1 H), 7.20 - 7.11 (m, 2 H), 6.90 - 6.80 (m, 2 H), 6.76 (s, 1 H), 4.23 - 4.16 (m, 1 H), 4.09 (t, *J* = 6.1 Hz, 2 H), 3.92 (dt, *J* = 4.6, 11.9 Hz, 1 H), 3.05 (dd, *J* = 5.2, 15.7 Hz, 1 H), 2.44 (dd, *J* = 11.0, 15.8 Hz, 1 H), 2.22 (s, 3 H), 2.20 - 2.10 (m, 2 H), 2.00 - 1.90 (m, 2 H), 1.79 - 1.72 (m, 1 H)

GDI-9198



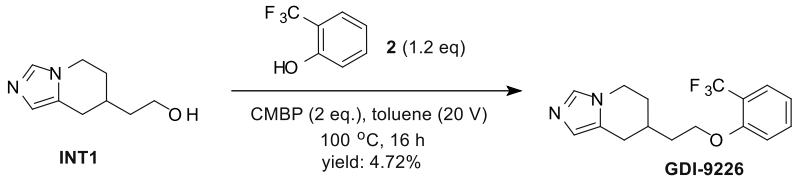
Synthesis of compound **GDI-9198**: compound **INT1** (40 mg, 192 μmol, 1 eq) and compound **2** (30 mg, 231 μmol, 1.2 eq) were dissolved in toluene (0.8 mL), and CMBP (93 mg, 385 μmol, 2 eq) were added at 25 °C. The reaction mixture was stirred at 100 °C for 16 hours under a nitrogen atmosphere, and reaction completion was confirmed by LCMS. The reaction mixture was concentrated under reduced pressure and purified via silica gel chromatography (SiO_2, EtOAc/MeOH = 10/1) followed by HPLC (column: Waters Xbridge BEH C18 100 × 30 mm, 10 μm; mobile phase: [H_2O (10 mM NH_4HCO_3)–ACN]; gradient: 38%–68% B over 8.0 min) to afford the target compound **GDI-9198** (5.1 mg, 18.1 μmol, 9.42% yield, 98.4% purity) as a white solid, ESI-MS: $[M+H]^+$, 277.10. **^{1}H NMR** (400 MHz, Chloroform-d_3) δ = 7.41 (s, 1 H), 7.37 (d, *J* = 7.8 Hz, 1 H), 7.26 - 7.18 (m, 1 H), 6.98 - 6.89 (m, 2 H), 6.76 (s, 1 H), 4.23 - 4.10 (m, 3 H), 3.93 (dt, *J* = 4.7, 11.8 Hz, 1 H), 3.06 (dd, *J* = 4.6, 15.8 Hz, 1 H), 2.45 (dd, *J* = 10.3, 15.8 Hz, 1 H), 2.19 (dd, *J* = 4.3, 9.3 Hz, 2 H), 2.04 - 1.91 (m, 2 H), 1.82 - 1.73 (m, 1 H)

GDI-9225



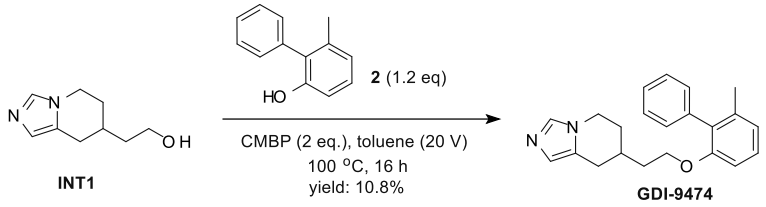
Synthesis of compound **GDI-9225**: **INT1** (40 mg, 240 μmol, 1 eq) and compound **2** (34.4 mg, 288 μmol, 1.2 eq) were dissolved in toluene (1 mL), and CMBP (116 mg, 481 μmol, 2 eq) were added at 25 °C. The reaction mixture was stirred at 100 °C for 16 hours under a nitrogen atmosphere, and reaction completion was confirmed by LCMS. The reaction mixture was concentrated under reduced pressure and purified via high-performance liquid chromatography (column: WePure Biotech XP tC18 150×40 mm, 70 μm; mobile phase: [H_2O (10 mM NH_4HCO_3)–ACN]; gradient: 20%–50% B over 8.0 min) followed by silica gel chromatography (SiO_2, EtOAc/MeOH = 10/1) to afford the target compound **GDI-9225** (10 mg, 37.4 μmol, 15.5% yield) as a yellow oil.ESI-MS: $[M+H]^+$, 268.1. **^{1}H NMR** (400 MHz, Chloroform-d_3) δ 7.60 - 7.51 (m, 2 H), 7.43 (s, 1 H), 7.03 (dt, *J* = 0.7, 7.6 Hz, 1 H), 6.98 (d, *J* = 8.5 Hz, 1 H), 6.77 (s, 1 H), 4.30 - 4.10 (m, 3 H), 3.97 (dd, *J* = 4.7, 11.4 Hz, 1 H), 3.10 - 2.99 (m, 1 H), 2.46 (dd, *J* = 10.3, 15.8 Hz, 1 H), 2.27 - 2.14 (m, 2 H), 2.09 - 2.02 (m, 1 H), 1.97 - 1.90 (m, 1 H), 1.78 (dd, *J* = 5.5, 13.9 Hz, 1 H)

GDI-9226



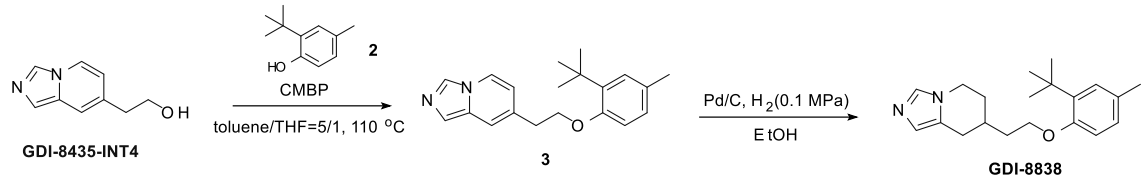
Synthesis of compound **GDI-9226**: **INT1** (40 mg, 241 μmol, 1 eq) and compound **2** (46.8 mg, 289 μmol, 1.2 eq) were dissolved in toluene (0.8 mL). CMBP (116 mg, 481 μmol, 2 eq) was added at 25 °C, and the reaction mixture was stirred at 100 °C for 16 hours under a nitrogen atmosphere, and reaction completion was confirmed by LCMS. The reaction mixture was concentrated under reduced pressure and purified via silica gel chromatography (SiO_2, EtOAc/MeOH = 10/1) followed by HPLC (column: Waters Xbridge BEH C18 100×30 mm, 10 μm; mobile phase: [H_2O (10 mM NH_4HCO_3)–ACN]; gradient: 38%–68% B over 8.0 min) to afford the target compound **GDI-9226** (3.9 mg, 11.4 μmol, 4.72% yield, 90.5% purity) as a yellow oil. ESI-MS: $[M+H]^+$, 311.1. **^{1}H NMR** (400 MHz, Chloroform-d_3) δ = 7.58 (d, *J* = 7.6 Hz, 1 H), 7.49 (d, *J* = 7.5 Hz, 1 H), 7.40 (s, 1 H), 7.05 - 6.97 (m, 2 H), 6.75 (s, 1 H), 4.18 (t, *J* = 6.0 Hz, 3 H), 3.91 (d, *J* = 4.5 Hz, 1 H), 3.03 (dd, *J* = 4.8, 15.7 Hz, 1 H), 2.43 (dd, *J* = 10.6, 15.8 Hz, 1 H), 2.23 - 2.09 (m, 2 H), 1.96 (td, *J* = 3.1, 6.2 Hz, 2 H), 1.75 (s, 1 H)

GDI-9474



Synthesis of compound **GDI-9474**: **INT1** (20 mg, 120 μmol, 1 eq) and compound **2** (26.6 mg, 144 μmol, 1.2 eq) were dissolved in toluene (0.4 mL), and CMBP (58.1 mg, 241 μmol, 2 eq) was added at 25 °C. The reaction mixture was stirred at 100 °C for 16 hours under a nitrogen atmosphere, and reaction completion was confirmed by LCMS. The reaction mixture was concentrated under reduced pressure and purified sequentially via silica gel chromatography (SiO_2, EtOAc/MeOH = 10/1) and high-performance liquid chromatography (column: Waters Xbridge BEH C18 100×30 mm, 10 μm; mobile phase: [H_2O (10 mM NH_4HCO_3)–ACN]; gradient: 38%–68% B over 8.0 min) to yield the target compound **GDI-9474** (4.3 mg, 12.9 μmol, 10.8% yield, 100% purity) as a yellow oil. ESI-MS: $[M+H]^+$, 333.1. **^{1}H NMR** (400 MHz, Chloroform-d_3) δ = 7.36 (s, 3 H), 7.26 - 7.14 (m, 3 H), 6.92 (d, *J* = 7.5 Hz, 1 H), 6.82 (d, *J* = 8.1 Hz, 1 H), 6.68 (s, 1 H), 4.08 - 3.91 (m, 3 H), 3.64 (dt, *J* = 4.7, 11.7 Hz, 1 H), 2.74 (dd, *J* = 3.4, 15.8 Hz, 1 H), 2.15 (dd, *J* = 9.1, 15.8 Hz, 1 H), 2.09 (s, 3 H), 1.80 - 1.59 (m, 5 H), 1.53 - 1.38 (m, 1 H)

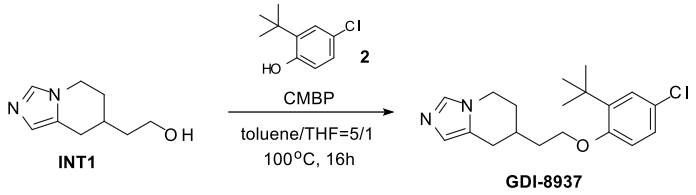
GDI-8838



Synthesis of compound **3**: a solution of **GDI-8435-INT4** (100 mg, 0.62 mmol), 2-tert-butyl-4-methylphenol (152 mg, 0.92 mmol) and CMBP (298 mg, 1.23 mmol) in toluene/THF (5 mL /1 mL) stirred under nitrogen at 110℃ for 16 hs, and reaction completion was confirmed by LCMS. The resulting mixture was diluted with water (20 mL) and extracted with EtOAc (20 mL * 3). The combined organic phases were washed with brine, dried over sodium sulfate, concentrated, and purified by silica gel column chromatography (eluting with MeOH/DCM, 2% to 5%) to give the pure product compound **3** (75 mg,0.24 mmol,39.44 % yield) as a yellow solid, ESI-MS: $[M+H]^+$, 309.

Synthesis of compound **GDI-8838**: a mixture of compound 3 (75 mg, 0.24 mmol) and Pd/C (13 mg, 0.12 mmol) in EtOH (5 mL) was stirred at 25℃ for 16 hours under an atmosphere of H_2 (0.1 Mpa). After the mixture was filtered through celite and the filtrate was concentrated under vacuum. Then the reaction mixture was concentrated in vacuo, the residue was further purified by prep-HPLC (Gemini 5 um C18 column, 150*21.2 mm, eluting with 10% to 20% ACN/H_2O containing) to give the **GDI-8838** (29.42 mg, 0.09 mmol, 38.73% yield) as a yellow solid, ESI-MS: $[M+H]^+$, 312.8. **^{1}H NMR** (400 MHz, DMSO-d_6) δ 7.46 (s, 1 H), 7.00 (s, 1 H), 6.96 (d, J = 8.3 Hz, 1 H), 6.88 (d, J = 8.2 Hz, 1 H), 6.59 (s, 1 H), 4.17 (m, 1 H), 4.05 (t, J = 6.6 Hz, 2 H), 3.82 (m, 1 H), 2.94 (m, 1 H), 2.37 (m, 1 H), 2.22 (s, 3 H), 2.04 (m, 2 H), 1.87 (m, 2 H), 1.63 (m, 1 H), 1.32 (s, 9 H).

GDI-8937



Synthesis of compound **GDI-8937**: a solution of **INT1** (80 mg, 0.48 mmol),2-tert-butyl-4-chlorophenol (133 mg, 0.72 mmol) and CMBP (232 mg, 0.96 mmol) in toluene/THF (5 mL /1 mL) stirred under nitrogen at 100℃ for 16H, and reaction completion was confirmed by LCMS. After that the solution was poured into H_2O (20 mL). The solution was extracted with EtOAc (20 mL * 3) and dried over Na_2SO_4, filtered and concentrated to give a residue. The residue was further purified by prep-HPLC (Gemini 5 um C18 column, 150*21.2 mm, eluting with 10% to 20% ACN/H_2O containing) to give the **GDI-8937** (36.94 mg,0.11 mmol,23.06% yield) as a yellow oil, ESI-MS: $[M+H]^+$, 333.05. **^{1}H NMR** (400 MHz, DMSO-d_6) δ 7.45 (s, 1 H), 7.18 (m, 2 H), 6.97 (d, J = 8.5 Hz, 1 H), 6.58 (s, 1 H), 4.13 (m, 3 H), 3.85 (m, 1 H), 2.93 (m, 1 H), 2.34 (m, 1 H), 2.13 (s, 3 H), 2.04 (d, J = 13.5 Hz, 2 H), 1.84 (m, 2 H), 1.64 (m, 1 H).

GAC15 and analogs general synthesis method: the carboxylic acid compound (1.32 mmol, 1.3 eq), TCFH (343 mg, 1.22 mmol, 1.2 eq), and NMI (251 mg, 3.06 mmol, 244 μL, 3 eq) were sequentially dissolved in DMF (2.6 mL), and the amine compound (1.02 mmol, 1 eq) was added at 25 °C. The reaction mixture was stirred at 25 °C for 16 hours, and reaction completion was confirmed by LCMS. Water (5 mL) was added to the reaction mixture, followed by extraction with EtOAc (3 mL * 3). The combined organic phases were concentrated under reduced pressure and purified sequentially via silica gel chromatography (SiO_2, petroleum ether/EtOAc = 1/1) and high-performance liquid chromatography (column: WePure Biotech XP tC18 150 × 40 × 7 μm; mobile phase: [H_2O (10 mM NH_4HCO_3)–ACN]; gradient: 30%–70% B over 8.0 min) to afford the target compound.

GAC15: ESI-MS: $[M+H]^+$, 280.85. **^{1}H NMR** (400 MHz, DMSO-d_6) δ 10.45 (s, 1 H), 8.67 (m, 2 H), 7.93 (s, 1 H), 7.68 (d, *J* = 8.3 Hz, 1 H), 7.41 (t, *J* = 8.1 Hz, 1 H), 7.20 (m, 1 H).

GAC15-11: ESI-MS: $[M+H]^+$, 238.04, **^{1}H NMR** (400 MHz, DMSO-d_6) δ 10.20 (s, 1 H), 8.37 (dd, *J* = 3.0, 1.3 Hz, 1 H), 7.94 (t, *J* = 2.1 Hz, 1 H), 7.71 – 7.64 (m, 2 H), 7.63 (dd, *J* = 5.1, 1.3 Hz, 1 H), 7.38 (t, *J* = 8.1 Hz, 1 H), 7.15 (ddd, *J* = 8.0, 2.2, 0.9 Hz, 1 H).

GAC15-12: ESI-MS: $[M+H]^+$, 252.02, **^{1}H NMR** (400 MHz, DMSO-d_6) δ 10.11 (s, 1 H), 8.10 (d, *J* = 1.5 Hz, 1 H), 7.93 (t, *J* = 2.1 Hz, 1 H), 7.67 (ddd, *J* = 8.3, 2.1, 1.0 Hz, 1 H), 7.37 (t, *J* = 8.1 Hz, 1 H), 7.32 (t, *J* = 1.4 Hz, 1 H), 7.14 (ddd, *J* = 8.0, 2.2, 0.9 Hz, 1 H).

GAC15-13: ESI-MS: $[M+H]^+$, 263.10,

GAC15-14: ESI-MS: $[M-H]^-$, 251.0. **^{1}H NMR** (400 MHz, DMSO-d_6) δ = 9.92 (s, 1 H), 7.91 (t, *J* = 2.0 Hz, 1 H), 7.65 (dd, *J* = 1.2, 8.2 Hz, 1 H), 7.34 (t, *J* = 8.1 Hz, 1 H), 7.23 (d, *J* = 1.5 Hz, 1 H), 7.11 (dd, *J* = 1.5, 7.9 Hz, 1 H), 6.34 (d, *J* = 1.5 Hz, 1 H), 5.71 (s, 2 H)

GAC15-15: ESI-MS: $[M+H]^+$, 315.92, **^{1}H NMR** (400 MHz, DMSO-d_6) δ 10.22 (s, 1 H), 8.34 (d, *J* = 1.6 Hz, 1 H), 7.91 (t, *J* = 2.1 Hz, 1 H), 7.73 (d, *J* = 1.7 Hz, 1 H), 7.66 (ddd, *J* = 8.2, 2.0, 1.0 Hz, 1 H), 7.38 (t, *J* = 8.1 Hz, 1 H), 7.17 (ddd, *J* = 8.0, 2.1, 0.9 Hz, 1 H).

GAC15-16: ESI-MS: $[M+H]^+$, 349.92, **^{1}H NMR** (400 MHz, DMSO-d_6) δ 10.32 (s, 1 H), 8.34 (d, *J* = 1.6 Hz, 1 H), 8.10 (d, *J* = 2.4 Hz, 1 H), 7.74 – 7.67 (m, 2 H), 7.62 (d, *J* = 8.8 Hz, 1 H).